Understanding changes in water availability in the Rio Grande/Río Bravo del Norte basin under the influence of large-scale circulation indices using the Noah land surface model

C. Prakash Khedun,[1] Ashok K. Mishra,[2] John D. Bolten,[3] Hiroko K. Beaudoing,[3,4] Ronald A. Kaiser,[1,5] J. Richard Giardino,[1,6] and Vijay P. Singh[1,2,7]

Received 21 July 2011; revised 15 November 2011; accepted 28 December 2011; published 3 March 2012.

[1] Water availability plays an important role in the socio-economic development of a region. It is however, subject to the influence of large-scale circulation indices, resulting in periodic excesses and deficits. An assessment of the degree of correlation between climate indices and water availability, and the quantification of changes with respect to major climate events is important for long-term water resources planning and management, especially in transboundary basins as it can help in conflict avoidance. In this study we first establish the correlation of the Pacific Decadal Oscillation (PDO) and El Niño-Southern Oscillation (ENSO) with gauged precipitation in the Rio Grande basin, and then quantify the changes in water availability using runoff generated from the Noah land surface model. Both spatial and temporal variations are noted, with winter and spring being most influenced by conditions in the Pacific Ocean. Negative correlation is observed at the headwaters and positive correlation across the rest of the basin. The influence of individual ENSO events, classified using four different criteria, is also examined. El Niños (La Niñas) generally cause an increase (decrease) in runoff, but the pattern is not consistent; percentage change in water availability varies across events. Further, positive PDO enhances the effect of El Niño and dampens that of La Niña, but during neutral/transitioning PDO, La Niña dominates meteorological conditions. Long El Niños have more influence on water availability than short duration high intensity events. We also note that the percentage increase during El Niños significantly offsets the drought-causing effect of La Niñas.

Citation: Khedun, C. P., A. K. Mishra, J. D. Bolten, H. K. Beaudoing, R. A. Kaiser, J. R. Giardino, and V. P. Singh (2012), Understanding changes in water availability in the Rio Grande/Río Bravo del Norte basin under the influence of large-scale circulation indices using the Noah land surface model, *J. Geophys. Res.*, *117*, D05104, doi:10.1029/2011JD016590.

1. Introduction

[2] Large-scale climate patterns have a significant influence on local atmospheric and hydrologic variables, and consequently on water availability. Several studies have investigated the influence of climate variability using either a single index or a combination of indices on precipitation [e.g., *McCabe and Dettinger*, 1999; *Piechota and Dracup*, 1996; *Ropelewski and Halpert*, 1986; *Woolhiser et al.*, 1993], streamflow [e.g., *Barlow et al.*, 2001; *Kahya and Dracup*, 1993; *Redmond and Koch*, 1991], and drought [e.g., *Özger et al.*, 2009; *Schoennagel et al.*, 2005] in the United States (U.S.). In the southern U.S., the Pacific Decadal Oscillation (PDO) and the El Niño-Southern Oscillation (ENSO) have been found to be the two most dominant climate teleconnections influencing regional hydrological conditions.

[3] ENSO is a coupled ocean-atmosphere phenomenon related to sea surface temperature (SST) anomalies (SSTA) in the central and eastern equatorial Pacific and associated sea level pressure difference known as the Southern Oscillation [*Rasmusson and Carpenter*, 1982]. It has a recurrence pattern of 3 to 6 years and every event normally lasts for about a year. El Niño events, the positive or warm phase of ENSO, are often, but not always, followed by La Niña

[1]Water Management and Hydrological Science, Texas A&M University, College Station, Texas, USA.
[2]Department of Biological and Agricultural Engineering, Texas A&M University, College Station, Texas, USA.
[3]Hydrologic Science Branch, NASA Goddard Space Flight Center, Greenbelt, Maryland, USA.
[4]Earth System Science Interdisciplinary Center, University of Maryland, College Park, Maryland, USA.
[5]Department of Recreation, Park and Tourism Sciences, Texas A&M University, College Station, Texas, USA.
[6]Department of Geology and Geophysics, Texas A&M University, College Station, Texas, USA.
[7]Department of Civil Engineering, Texas A&M University, College Station, Texas, USA.

0148-0227/12/2011JD016590

events, also referred to as the negative or cold phase of ENSO. More recently, a new type of El Niño, occurring more frequently, with inter-annual variability, has been observed [*Ashok et al.*, 2007]. It has been named El Niño Modoki (Japanese for "similar but different"). It occurs with a shift in the warming center from the eastern equatorial Pacific, which is the case with regular El Niño, to central equatorial Pacific, and both the eastern and western regions are flanked by anomalously cool temperatures, thus resulting in an SST gradient that generates a two-cell Walker Circulation in the troposphere with a wet region over the central Pacific. When coupled with other ongoing atmospheric disturbances, a dry rim arises around the wet central tropical Pacific. Given the similarities between canonical ENSO and this new occurrence, it is easy to confuse between their impacts. Partial correlation and regression analyses suggest that they are distinct phenomena in both space and time and do not appear as an evolving phase of one or the other [*Weng et al.*, 2007].

[4] PDO is a long-lived El Niño-like pattern of Pacific climate variability with a cycle of about 20 to 30 years [*Mantua and Hare*, 2002]. PDO influences the hydrological cycle in the same way as ENSO, but with more pronounced influence in the extra tropics and secondary influence in the tropics. The similarities in the signature between ENSO and PDO have led to the hypothesis that the two teleconnections may be related, or PDO may be forced by ENSO [*Zhang et al.*, 1997]. Statistical analysis by *Newman et al.* [2003] showed that PDO is dependent on ENSO on all timescales. When the PDO is in its positive or warm phase, above normal SST is observed along the west coast of North America and below normal SST along the central and western North Pacific around 45°N. The Aleutian low strengthens and winter precipitation increases in the southern U.S. [*Mantua et al.*, 1997].

[5] Recently *Kurtzman and Scanlon* [2007] examined the impacts of ENSO and PDO on winter precipitation in 165 climate divisions in southern and central U.S. and found a significant increase (decrease) with respect to El Niño (La Niña). The correlation with PDO was weaker, but when both indices were combined, it was noted that La Niñas occurring during the cold phases of PDO exhibited strong influence in central U.S. and El Niños occurring during the warm phases of PDO dominated southwest and southeast United States. *Redmond and Koch* [1991] noted that if events in the Pacific Ocean are causally related to remote meteorological variables, it would be separated by a time lag. They found statistically significant correlations with lags ranging between 0 to 6 months between the Southern Oscillation Index (SOI) and precipitation in the western United States. *Kumar and Hoerling* [2003] found that the maximum correlation between observed zonal mean tropical 200-mb heights and SST in the Pacific occurs with a lag of 1 to 3 months and this results in a lag of one season between rainfall in the tropical Pacific and Niño 3.4 SSTA. The robustness of these results was confirmed using an atmospheric general circulation model (GCM).

[6] While these information, on the degree of association between hydrologic variables and climate patterns, are valuable, they are only of qualitative nature and their use in water management is limited. Water planning and management is driven by demand, priority, and availability. Demand is influenced by demographic and economic changes, while priority is an institutional variable defined by legal, social, and economic constraints. Availability, on the other hand, is a natural variable subjected to the whims of climate.

[7] In this paper we investigate the influence of large-scale climate indices, namely ENSO and PDO, on the water availability within the Rio Grande/Río Bravo del Norte basin (RG). RG is a transboundary basin shared between three states in the U.S. and straddles U.S. and Mexico, two countries very dissimilar economically. It is a vital source of water for the region, but is already in a state of absolute water scarcity, with less than 500 m^3/person/day; the only transboundary basin in this category [*Wolf*, 2002]. This region is also extremely vulnerable to droughts; records show that it suffers from both short-term and long-term droughts [*Quiring and Goodrich*, 2008]. Subjected to a burgeoning population, which will further increase the stress on water allocation, and climate change, which will likely result in a decrease in precipitation [*Intergovernmental Panel on Climate Change*, 2007], the potential for conflicts cannot be overlooked. It is therefore imperative to understand the mechanisms driving water availability and quantify any change for long-term sustainable water planning and management.

[8] The study is divided into two main sections. We first establish the correlation between large-scale circulation indices and gauged precipitation to explore the spatial and temporal influence of ENSO and PDO separately on the basin. The correlation structure of precipitation with two canonical ENSO indices (Niño 3.4 and the Multivariate ENSO index (MEI)) were compared to that of the El Niño Modoki index (EMI) to determine which index shows maximum correlation and is best suited for water management within the basin.

[9] Runoff is not linearly related to precipitation, but affected by natural processes and subjected to other meteorological variations such as temperature, evapotranspiration, wind speed, etc. which are also influenced by remote climate teleconnections. Streamflow is often used as a measure of surface water availability, but in large basins, stream gage records are not a realistic representation of actual flow as they are affected by dams, diversions, return flows, reduction in base flows by excessive groundwater pumping, and urbanization [*Legates et al.*, 2005], thus obscuring climate influences. We therefore use a land surface model (LSM), but keep land-use-land-cover constant, to generate runoff as it incorporates all necessary factors in the process. The basin is divided into six sub-regions and the temporal variations in water availability with respect to climate indices are examined.

[10] El Niño (La Niña) events are not similar and coincide with different phases of PDO (positive, negative, or transitioning from one phase to another). We compare and rank individual El Niño and La Niña events based on their durations, maximum (or minimum) SSTA recorded, and intensities – a new metric that we propose in this study. The percentage change in water availability in each sub-region, with respect to individual El Niño and La Niña events and coincident PDO phases is then examined.

[11] The paper is organized as follows. Section 2 discusses the methodology and the choice of LSM adopted for this

study. A description of the study basin is given in section 3. Section 4 describes the data sets for precipitation and climate indices, and forcing and parameters for the LSM. The first part of section 5 discusses the hydroclimatology of the basin, the correlation between climate indices and gauged precipitation, and the differences between ENSO events. In the second part we discuss the model output and validation, and investigate the lags and changes in water availability with respect to climate variability. The main conclusions drawn from the study are given in section 6.

2. Methodology

[12] Pearson correlation is used to determine the relationship between climate indices and gauged seasonal precipitation data. Kriging interpolation is employed to map the spatial variation of the correlation coefficient across the study area. Runoff, which is a proxy for surface water availability, is obtained from an LSM. The factors considered in the selection of the most appropriate LSM for the region is discussed. Continuous wavelet transform is used to investigate the temporal structure and influence of climate variability on water availability.

2.1. Correlation

[13] The Pearson correlation coefficient, ρ_{xy}, is a measure of linear association between two time series: x and y. The lag-correlation coefficient, $\rho_{xy}(k)$, is the cross-correlation for lag k between the time series. The range for $\rho_{xy}(k)$ is $[-1, 1]$, with larger $|\rho_{xy}|$ implying greater ability of x to predict y [*von Storch and Zwiers*, 2003]. The correlation coefficient can be used as a statistical test of independence to help make inferences about the degree of association between variables. The null hypothesis is that the two time series are independent and identically distributed (iid) normal random variables ($\rho_{xy} = 0$).

2.2. Land Surface Modeling

[14] LSMs compute terrestrial water, energy, momentum, and bio-geochemical exchange processes by solving the governing equations of the soil-vegetation-snowpack medium [*Peters-Lidard et al.*, 2007]. A number of LSMs have been developed over the last 30 years and are constantly being refined as our understanding of the physics underlying earth system processes improves, and computing capabilities increases. Four LSMs, namely Mosaic, Noah, the Variable Infiltration Capacity (VIC), and Sacramento models, were evaluated over the Continental U.S. (CONUS) as part of the North American Land Data Assimilation System (NLDAS) project [*Mitchell et al.*, 2004]. *Lohmann et al.* [2004] evaluated these models for their performance in partitioning water balance terms (evapotranspiration, runoff, and storage change) across four different quadrants over CONUS, and their ability to reproduce streamflow at different timescales (daily, monthly, and annual) and noted that at the continental scale the results varied significantly in the wet eastern U.S. but were generally in agreement over the drier western region. The Mosaic and Sacramento models underestimate runoffs, and VIC produced more runoff, while Noah's predictions fell in between. In small- to medium-sized catchments, the models showed similar bias gradients in the east, increasing from north to south. VIC, for example, produced the right annual runoff in the northeast U.S. but more runoff toward the south. Noah predicts less runoff in the northeast U.S., more in the south, and the right runoff in the middle.

[15] Noah was also found to exhibit the lowest regional bias. *Lohmann et al.* [2004] further speculated that the high runoff produced by the models in the southwestern U.S. may be attributed to farming and irrigation which is not included within the NLDAS setup. Seasonal analysis showed that Noah produced correct runoff in a number of basins for the cold season with the same north-south annual bias. Both VIC and Noah produced soil moisture anomalies close to observed values. However, in the Little River Experimental Watershed, *Sahoo et al.* [2008] found that Noah produced higher soil moisture, which, as a result of the model physics governing partitioning, produced less surface and subsurface runoff. Nevertheless *Lohmann et al.* [2004], found that the Sacramento and Noah reproduced daily streamflow better, with Noah having the highest overall score based on the Nash-Sutcliff efficiency. The study also evaluated the model performance over nine large basins in the United States. RG was not included, but the sizes of the basins examined are comparable. There was disagreement between modeled and measured runoff in high and less regulated basins. In high regulated basis, which comprise a number of dams and reservoirs, smaller seasonal signals were observed, whereas in less regulated ones, seasonality was closely captured. This confirms that the models were actually effectively reproducing seasonal variations, which is being dampened by engineering infrastructures in the highly regulated basins, thus lending credence in using an LSM in modeling RG which has a large number of dams, diversions, and reservoirs.

2.2.1. Noah LSM

[16] The community Noah LSM's [*Chen et al.*, 1996; *Koren et al.*, 1999] legacy extends into modeling efforts carried in the 1980s [*Mahrt and Ek*, 1984; *Mahrt and Pan*, 1984; *Pan and Mahrt*, 1987] and has been further refined in the 1990s under the GEWEX/GCIP/GAPP Program Office of NOAA/OGP, led by the National Centers for Environmental Prediction (NCEP) and benefitting from the collaboration of investigators from both public and private institutions. Noah has been a candidate in major off-line land surface experiments, such as the Project for Intercomparison of Land-surface Parameterization Schemes (PIPLS) [*Henderson-Sellers et al.*, 1996] and the Global Soil Wetness Project (GSWP) [*Dirmeyer et al.*, 1999] among others. It has been validated in both coupled and uncoupled modes [*Mitchell*, 2005].

[17] Noah is a stand-alone 1-D column model that can simulate soil moisture (both liquid and frozen), soil temperature, skin temperature, snowpack depth, snowpack water equivalent, canopy water content, and water and energy flux terms of the surface water and energy balance [*Mitchell*, 2005]. The model has a snow layer and a canopy layer. The soil profile extends to a depth of 2 m divided into four layers from the ground surface to the bottom: 0–0.1 m, 0.1–0.4 m, 0.4–1 m, and 1–2 m. The root zone is limited to the upper 1 m of soil, and the lower 1 m layer acts as a reservoir with gravity drainage at the bottom. The snow layer simulates snow accumulation, sublimation, melting, and heat exchange at snow-atmosphere and snow-soil

interfaces. Precipitation is deemed snow if the temperature of the lowest atmospheric layer is below 0°C. The total evaporation, in the absence of snow, is the sum of direct evaporation from the topmost soil layer [*Mahfouf and Noilhan*, 1991], evaporation of precipitation intercepted by plant canopy, and transpiration from canopy of vegetation [*Jacquemin and Noilhan*, 1990; *Noilhan and Planton*, 1989]. Surface runoff is the excess after infiltration [*Schaake et al.*, 1996]. A complete description of the model physics and order in which computations are carried out is provided by *Chen and Dudhia* [2001].

[18] *Lohmann et al.* [2004] point out that one notable difference between Noah and other LSMs considered in the NLDAS project is the earlier onset of runoff in snowmelt season when compared to other models and observed values. This may make Noah a less likely candidate for streamflow studies in snow dominated watersheds. In Noah, snow can either sublimate or melt as there is no horizontal transport. *Sheffield et al.* [2003] and *Pan et al.* [2003] evaluated the four LSMs considered in the NLDAS project for snow cover extent and simulated snow water equivalent. Systematic low biases were observed in the snow cover extent and snow water equivalent in the simulations for all four models and larger discrepancies were observed at higher elevations. Noah consistently underestimates the snow cover extent at all elevations. This under-prediction is partly explained by its higher snow water equivalent threshold for large snow cover values as compared to other models. Noah also tends to melt snow earlier, which is due to the low albedo values in each snow covered grid, which leads to higher available energy at the surface creating a positive feedback mechanism which enhances snowmelt and sublimation.

[19] *Hogue et al.* [2005] evaluated the transferability of calibrated parameters in Noah between two semi-arid sites in the southern U.S. for evaluating model performance under the different climatic conditions these regions are subjected to. They found that generally Noah accurately simulated sensible heat, ground heat, and ground temperature. However, discrepancies were noted during brief periods of moist air influx responsible for monsoon or during El Niño. When compared against other LSMs, Noah reproduced streamflow with high accuracy, with the smallest bias in both evaporation and runoff with respect to observed annual water budget [*Mitchell et al.*, 2004].

[20] Thus, based on extensive evaluation and comparison and despite some of its limitations, Noah seems the best suited LSM for the hydrological modeling of RG for purposes of this study. This study also provides an opportunity to test the validity of Noah outside the southern U.S. border, while still within NLDAS-2 domain, and may thus supplement previous findings.

2.2.2. Land Information System

[21] Noah LSM was run within NASA Goddard Space Flight Center's (GSFC) Land Information System (LIS; http://lis.gsfc.nasa.gov/). LIS, designed as a problem solving environment for hydrologic modeling applications, is an integrated high-performance land surface modeling and data assimilation framework [*Kumar et al.*, 2006; *Peters-Lidard et al.*, 2007] which evolved from the Global Land Data Assimilation System (GLDAS) [*Rodell et al.*, 2004] and the North America Land Data Assimilation System (NLDAS) [*Mitchell et al.*, 2004].

2.3. Continuous Wavelet Transform

[22] Wavelet transform decomposes a signal in terms of some elementary functions derived from a "mother wavelet" using a sliding window function whose radius increases in space (i.e., decreasing in frequency), allowing the low-frequency content of the signal to be resolved [*Rivera et al.*, 2004]. A number of mother wavelets are commonly used, and can be grouped into continuous and orthogonal wavelets; each having intrinsic advantages for specific applications. We chose the Morlet wavelet, which consists of a plane wave modified by a Gaussian envelope, as it is the most widely used continuous wavelet in geophysical applications. Its complex structure allows the detection of both time-dependent amplitude and phase for different frequencies in the time series [*Lau and Weng*, 1995].

[23] *Kumar and Foufoula-Georgiou* [1997] discussed the applications of wavelet to geophysical processes. *Torrence and Compo* [1998] reported on the application of wavelet, including a comparison to the widowed Fourier transform, to climate analysis using ENSO series. *Labat et al.* [2001] showed how wavelet can be appropriately employed in rainfall-runoff analysis.

3. Study Area

[24] RG is the fifth longest river in North America. It originates in the snow dominated San Juan range in the Rocky Mountains in southern Colorado, at an altitude of around 3,700 m amsl, and flows through arid/semi-arid plains in a southeastward direction over a distance of approximately 3,100 km before discharging into the Gulf of Mexico. The basin encompasses an area of 557,722 km^2 straddling three states in the U.S. and five states in Mexico (Figure 1). The river catchment is narrow, with its length being considerably longer than its width, and has a dendritic drainage pattern. The watershed contains a number of endorheic sub-basins, such that only 468,374 km^2 (242,994 km^2 on the U.S. side and 225,380 km^2 on the Mexican side) actually contribute to flow in the river [*Patiño-Gomez*, 2005].

[25] Winter precipitation and spring runoff sustain flow in the basin. The flow is impounded in a number of dams and regulated by major diversions. Elephant Butte Dam in southern New Mexico supports agricultural production in the region. The release from the dam is apportioned between the U.S. and Mexico under the 1906 Convention for the Equitable Distribution of Waters of the Rio Grande [*International Boundary and Water Commission*, 1906]. From El Paso to Ojinaga/Presidio the river flows through one of its driest stretches [*U.S. Army Corps of Engineers*, 2008]. At El Paso (station 45 in Figure 2), for example, the mean annual rainfall is 219 mm, while the yearly pan evaporation is around 1,500 mm. At Ojinaga/Presidio, RG is regenerated from flow from the Río Conchos, which is one of its most important tributaries, originating in the Sierra Madre Occidental in northwestern Mexico at around 3,500 m amsl. Two international reservoirs, Amistad and Falcon, store and apportion the water between the U.S. and Mexico. Without any dam or diversion along its course, the virgin flow of RG is estimated at above 100 m^3/s [*Revenga et al.*, 2003]. However, the anthropogenization of the basin has constantly impacted flow, such that the actual mean historical

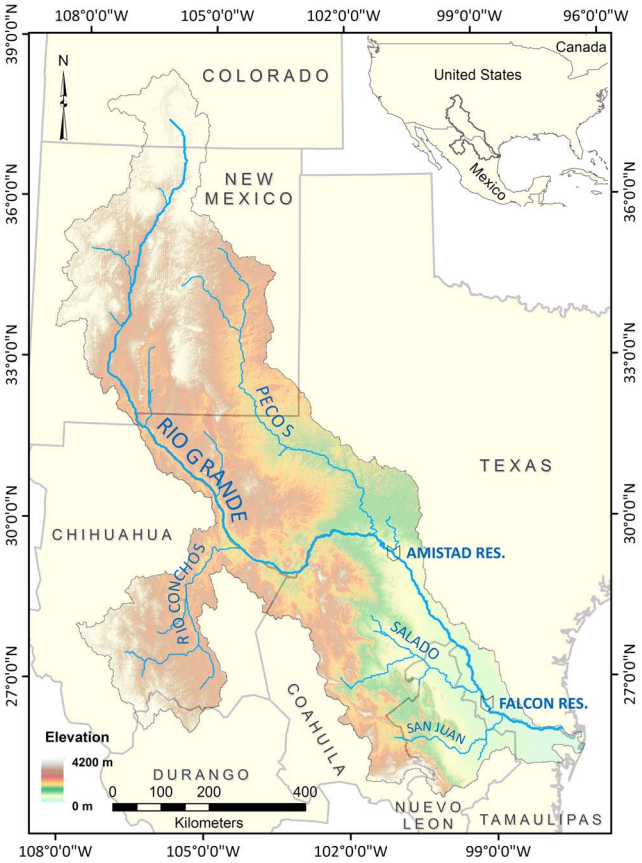

Figure 1. The Rio Grande/Río Bravo del Norte basin.

flow is 37 m^3/s, but in recent years the flow in the river has reduced considerably, and on several occasions the river failed to reach the sea.

[26] Land cover in RG is mainly desert shrubland and grassland, covering about 81%, while irrigated agriculture constitutes only 2.6% of the basin, and urban and industrial area covers 6% of the basin [*Revenga et al.*, 2003].

[27] Given its size, the varied climatology it is subjected to, and the major dams and diversions partitioning the system, RG cannot be studied as one watershed, nor can it be divided into sub-basins, as some tributaries, like the Pecos, runs along the main stem, crossing several latitudes, thus subjected to different climate teleconnection influences. Higher snowfall at the headwaters for example does not necessarily result in higher flow into the international reservoirs or at the mouth. Moreover, climate divisions from one U.S. state do not align with that from another state. The basin is therefore divided into six sub-regions (Figure 2) by considering the latter constraints and other geomorphological features in the system.

4. Data

4.1. Precipitation

4.1.1. United States

[28] The National Climatic Data Center (NCDC) has an extensive archive of publicly available weather data from NOAA's Cooperative Observer Program (COOP) stations in the United States. The COOP data contains gaps and only a few stations have continuous records. NCDC also houses the United States Historical Climatology Network (USHCN) version 2 data set which is a designated subset of the COOP network [*Karl et al.*, 1990]. The data set undergoes extensive quality control including adjustment for any time-of-observation bias. Only 27 stations out of the 1,221 stations in the USHCN are serially complete [*McRoberts and Nielsen-Gammon*, 2011], while missing data in the others have been filled using a weighted average of values from highly correlated neighboring stations. However, the density of the USHCN network is not adequate within RG for purposes of this study (see Figure 1 of USHCN Version 2 Serial Monthly Data set, available from http://www.ncdc.noaa.gov/oa/climate/research/ushcn/, which shows the distribution of both COOP and HCN sites).

[29] *McRoberts and Nielsen-Gammon* [2011] proposed the full network estimated precipitation (FNEP, available from http://atmo.tamu.edu/osc/fnep) which utilizes as many COOP observations from the network of more than 24,000 stations and an inverse distance weighting scheme, using stations that have at least 10 years of overlap data and highest correlation, to fill missing data and extend the record, thus creating a continuous series from 1895 to present. There are a total of 332 FNEP stations within the U.S. portion of RG, but only those that have a sufficiently long record of observational data, while ensuring adequate spatial coverage, were chosen, hence taking advantage of the filled gaps. The time period considered in the analysis is

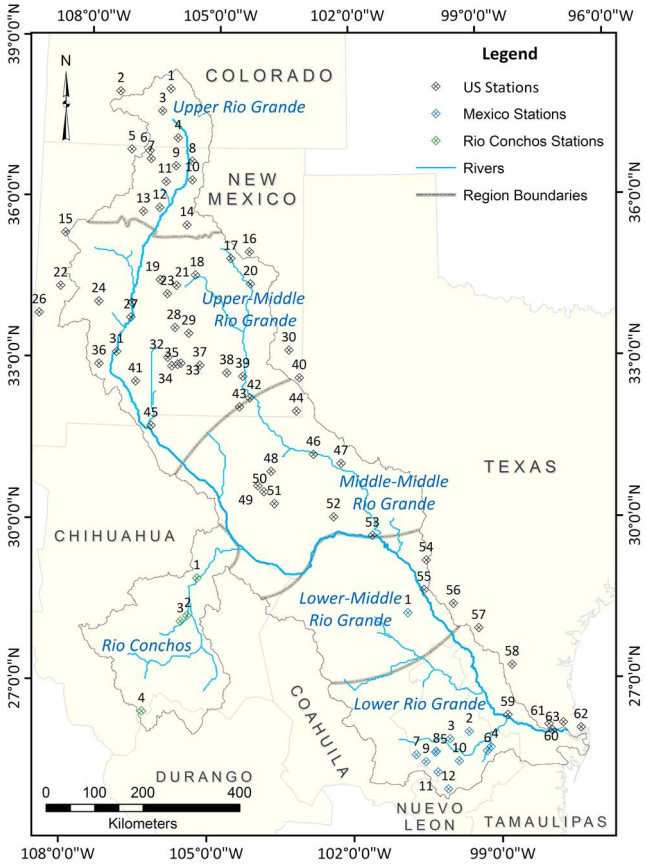

Figure 2. Location of precipitation stations used in this study.

January 1935 to December 2008, thus giving 74 years of data. Figure 2 shows the spatial distribution of the 63 stations (4 in Colorado, 40 in New Mexico, and 19 in Texas) selected.

4.1.2. Mexico

[30] Historical monthly precipitation data for the Mexican section of the basin was obtained from the Servicio Meteorológico Nacional (SMN), Comisión Nacional del Agua (CONAGUA), Mexico. SMN is the state entity responsible for the observation, recording, interpretation and dissemination of weather information in Mexico. The most updated observational data set obtained contained data up to December 2006 only, and any record beyond that date is not yet publicly available. For the Río Conchos sub-basin the latest available data is only up to December 2003.

[31] Of all the stations within the Mexican section of the basin, excluding the Río Conchos, 52 are operational and have records that extend up to 2006. However, most of these stations are very recent and only a few have records of at least 50 years, but have several years of missing data. A careful selection of viable stations, while ensuring maximum possible coverage, limited the number of stations that can be used in the study to only 12. The time period extended from January 1954 to December 2006. Records show that 9 stations are operational in the Río Conchos, but only 4 had sufficiently long records, extending from 1964 to 2003, for this study. Gaps were filled from neighboring stations that had sufficient amounts of overlapping data with the target stations. Any data missing from both the target and neighboring stations were filled with the long-term monthly mean. The spatial distribution of the selected stations is shown in Figure 2.

4.2. Climate Indices

4.2.1. Pacific Decadal Oscillation (PDO)

[32] Monthly PDO indices for the period 1935 to 2008 were obtained from the Joint Institute for the Study of the Atmosphere and Ocean (JISAO, http://jisao.washington.edu/pdo/PDO.latest). The PDO index is defined as the leading principal component of the North Pacific, poleward of 20°N, mean monthly SSTA [*Mantua et al.*, 1997]. The data is not influenced by global warming trends as monthly mean global average SSTA have been removed. A plot of the monthly indices, with a centered 13-month moving average to highlight multidecadal frequency is given in Figure 3. Positive (negative) values indicate warm (cold) phases of PDO. Between 1935 and 2008, 51% of warm months and 49% of cold months were recorded.

[33] Independent studies have shown two full PDO cycles in the last century [*Mantua and Hare*, 2002; *Minobe*, 1997], cool regimes that lasted from 1890 to 1924 and from 1947 to 1976, and warm phases that lasted from 1925 to 1946 and from 1977 to 1998. From 1998, PDO has been in a cold phase until 2002 and in a warm phase from 2002 to 2007. Occasional shifts, within the 20–30 year cycle, from cool (warm) to warm (cool) are visible in the record.

4.2.2. Niño 3.4

[34] There are four Niño regions along the equatorial Pacific, chosen in the early 1980s to describe and monitor SST. The warming across this region is not uniform and no single region can capture the whole ENSO phenomenon. *Bamston et al.* [1997] proposed the Niño 3.4 index as one that has both maximum correlation with the core ENSO phenomenon and strongest influence on remote teleconnection events. It is the area-averaged SSTA over the region bounded by 5°N–5°S and 120°W–170°W, straddling the Niño 3 and Niño 4 regions. Monthly data for the Niño 3.4 index was obtained from the International Research Institute (IRI) on Climate and Society Data Library (http://iridl.ldeo.columbia.edu/SOURCES/.Indices/.nino/.EXTENDED/). Figure 3 gives a plot of the Niño 3.4 index.

4.2.3. Multivariate ENSO Index (MEI)

[35] MEI is not based solely on SST but is a multivariate index based on six variables recorded over the tropical Pacific and published in the Comprehensive Ocean-atmosphere Data Set (COADS): sea level pressure, zonal and meridional components of the surface wind, sea surface temperature, surface air temperature, and total cloudiness fraction of the sky. It is the first unrotated principal component of all the six observed fields combined [*Wolter and Timlin*, 1993], and is analyzed separately for twelve sliding bi-monthly seasons, which removes most intraseasonal noise. For correlation studies, it is advised that the MEI values for month $(i - 1)$ and month (i) be treated as for month (i). Monthly data for MEI for 1950 to 2008 was obtained from NOAA's Earth System Research Laboratory (http://www.esrl.noaa.gov/psd//people/klaus.wolter/MEI/mei.html). Figure 3 gives a plot of the MEI.

4.2.4. El Niño Modoki (EMI)

[36] EMI is available from the Japan Agency for Marine-Earth Science and Technology (http://www.jamstec.go.jp/frcgc/research/d1/iod/modoki_home.html.en). It is defined as

$$EMI = [SSTA]_C - 0.5[SSTA]_E - 0.5[SSTA]_W \quad (1)$$

where [SSTA] is the area-averaged SST anomaly for the following regions: C (central, 165°E–140°W, 10°S–10°N), E (eastern, 110°W–70°W, 15°S–5°N), and W (western, 125°E–145°E, 10°S–20°N) [*Ashok et al.*, 2007]. The time series for EMI is given in Figure 3.

4.3. Forcing Data and Parameters for LSM

[37] The North American Land Data Assimilation System – Phase 2 (NLDAS-2) forcing data was used to run the Noah LSM. NLDAS-2 has a 1/8° latitude/longitude resolution over a domain covering CONUS, part of Canada and Mexico (125°W–67°W, 25°N–53°N), thus allowing the modeling of both the U.S. and Mexican portions of RG. It incorporates both measured and modeled data from multiple sources: gauged precipitation measurements, satellite data, radar precipitation measurements, and output from numerical prediction models. NLDAS has been run retrospectively starting in January 1979, and provide hourly measurements in near real-time. The data set include u and v wind components at 10 m above the surface, air temperature and specific humidity at 2 m above the surface, surface pressure, surface downward longwave and shortwave radiation, and total and convective fraction of precipitation, convective available potential energy, and potential evaporation.

[38] The precipitation field is from NCEP Climate Prediction Center (CPC) reprocessed daily gauged analyses that have been subjected to orographic adjustment based on the Parameter-elevation Regressions on Independent Slopes Model (PRISM) [*Daly et al.*, 1994] climatology and

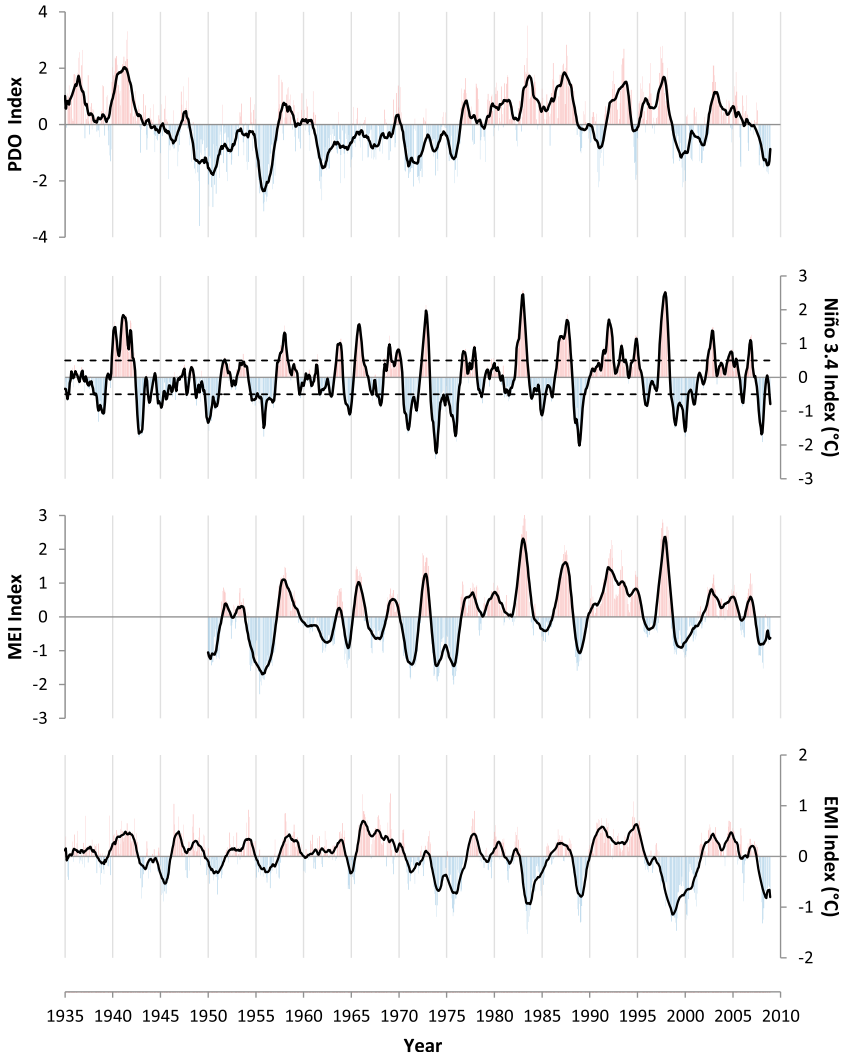

Figure 3. Time series of PDO, Niño 3.4, MEI, and EMI indices. The PDO, MEI, and EMI series are overlain with a running, centered 13-month average to highlight yearly variations. The normalized monthly Niño 3.4 index series is overlain with a centered 3-month running mean and ±0.5°C thresholds (see section 5.3.1).

interpolated to the 1/8° NLDAS grid, and temporally disaggregated to hourly timescale using either the NWS Doppler radar-based (WSR-88D) precipitation, which has a 4 km spatial coverage, or the 8 km NOAA CPC Morphing Technique (CMORPH) hourly precipitation analyses [*Joyce et al.*, 2004]. This product uses hourly multiagency gauge data for bias correction and has been mosaicked over CONUS by NCEP/EMC [*Baldwin and Mitchell*, 1997]. The radar network is limited at the U.S. borders with Canada and Mexico, and around 13% of CONUS are not covered. These gaps are first filled with nearest neighbor mosaicked data from within a 2° radius, and if the latter is not available, CMORPH data are used instead. In Mexico, which is outside the radar covering range, CMORPH data is used. CMORPH is not available before 2002, and CCP hourly data is used and if it is not available, the North American Regional Reanalysis (NARR) [*Mesinger et al.*, 2006] data is used instead.

[39] The NLDAS data set has been extensively compared, tested, and validated for snow cover and snow water equivalent [*Pan et al.*, 2003; *Sheffield et al.*, 2003], soil moisture [*Schaake et al.*, 2004], and streamflow and water balance [*Lohmann et al.*, 2004]. It has also been evaluated against the Atmospheric Measurement Program/cloud and radiation testbed, the Surface Radiation observation data, and the Oklahoma Mesonet, which is a quality controlled data set from a dense network of over 100 meteorological stations with meteorological measurements taken every 5 min [*Luo et al.*, 2003; *Robock et al.*, 2003].

[40] Noah also requires a set of parameters defining soil, vegetation, and topography for each grid. We use Zobler's assessment of Food and Agriculture Organization (FAO) Soil Units [*Zobler*, 1986] which gives sand, silt, and clay fractions. The land cover is from the University of Maryland's (UMD) 1 km spatial resolution global land cover product [*Hansen et al.*, 2000]. It contains 14 different classes (11 vegetation types, bare ground, urban/built up area, and

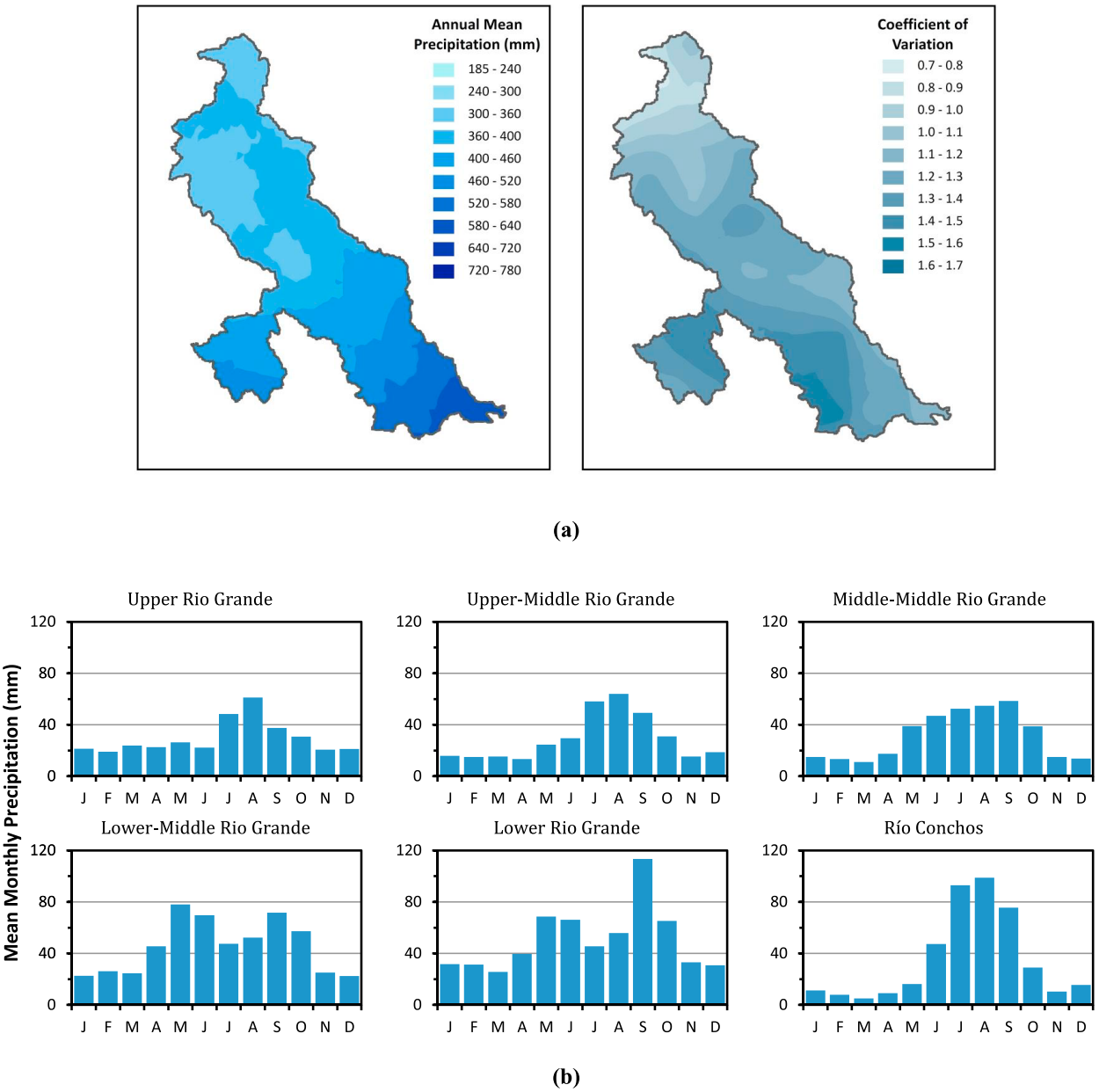

Figure 4. (a) Isohyet of annual mean precipitation and coefficient of variation of monthly precipitation across the Rio Grande basin, and (b) mean monthly precipitation for each region.

water). The model also requires information on the quarterly and maximum albedo, monthly greenness fraction, and bottom temperature without elevation corrections.

5. Results and Discussion

5.1. Hydroclimatology of the Basin

5.1.1. Spatial Variation

[41] RG trends across different climatic zones – alpine in southern Colorado and northern New Mexico, desert in southern New Mexico and west Texas, humid continental in east Texas, and humid sub-tropical in south Texas and northeastern Mexico [*Dahm et al.*, 2005] – making it an interesting study basin from both a hydrological and ecological perspective. Average annual precipitation varies from northwest to southeast across the basin, with a minimum of 187 mm at Manassa, in the San Juan Mountains, and a maximum of 698 mm at Port Isabel at the mouth of the basin. In the Río Conchos sub-basin, precipitation varies from southwest to northeast with a maximum annual mean of 781 mm at El Vergel, in the Sierra Madre Occidental, and a minimum of around 290 mm around the mouth as it discharges into RG. Figure 4 shows the isohyet of the annual mean precipitation and the coefficient of variation (C_v) of monthly precipitation across the basin. C_v is a statistical measure of variability, where a $C_v < 1$ indicates less variation, while a $C_v > 1$ indicates high variability.

[42] The basin exhibits wide disparity in precipitation regime, with C_v ranging between 0.7 and 1.7. The Upper RG region has low variability. It receives around 20 mm of precipitation every month except for JAS with August being the wettest month (Figure 4b). The middle portion of the basin exhibits high variability. It has a unimodal precipitation regime, typical of the southwestern U.S. where, for most of the year the average precipitation is below 20 mm except for May/June to September/October when the North American monsoon (NAM) brings most of the yearly rainfall. Río Conchos follows a similar pattern. NAM is a regional-scale circulation that develops over southwest North America, bringing substantial rainfall to this otherwise arid region. It is associated with a subtropical ridge shifting poleward during the summer months over the northwestern Mexican plateau and southwestern United States. As evidenced in the mean monthly precipitation distribution (Figure 4b) of the Río Conchos basin, the Upper-Middle and Middle-Middle RG, NAM starts to develop in late May to early June in southern Mexico quickly spreading along the western slopes of the Sierra Madre Occidental and into New Mexico and the western edge of Texas in early July and into southwestern U.S. in the middle of July and decays in September/October [*Adams and Comrie*, 1997; *Higgins et al.*, 1997]. The strength and path of the subtropical ridge is influenced by ENSO conditions. El Niño (La Niña) influences NAM by causing a weaker (stronger) southward (northward) displaced monsoon ridge [*Castro et al.*, 2001]. The lower part of the basin has a slightly bimodal precipitation pattern with May and June and September and October as the two wettest periods. Atlantic hurricanes bring copious amounts of rainfall in a very short period of time, often resulting in major flooding in this region. A strong relationship between ENSO and the frequency of Atlantic hurricanes has been noted, with El Niño (La Niña) favoring a decrease (increase) in activity [*Pielke and Landsea*, 1999].

5.1.2. Temporal Variation

[43] Figure 5 shows the time series of the average monthly precipitation from all stations within each region, smoothed with a centered 13-month moving average window to accentuate yearly variations. Precipitation from Mexican stations in Lower RG is shown in a separate plot. The top panel of the figure shows the duration of PDO and ENSO in their respective phases. Yearly standardized anomaly, which is the anomaly for a particular year divided by the standard deviation of the series, was calculated for each station. A positive (negative) standardized anomaly indicates higher (lower) than average precipitation. The patterns give a visual picture of the time, duration, and spatial extent of deficits and excesses in yearly precipitation across the basin. The standardized anomaly for the stations in the U.S., Mexico, and Río Conchos are shown separately in Figure 6.

[44] Precipitation across the basin varies both spatially (Figure 4) and temporally. The standardized anomaly plot shows that precipitation is generally around the long-term mean interspersed with drought spells, and a few extremely wet years, often spreading across the whole watershed. There have been more periods of rainfall deficits than excesses between 1935 and 2008. The most critical drought event started in 1951 and lasted up to 1956. In the semi-arid upper half portion of the basin, the drought started earlier, in 1942, right after an exceptionally wet year (1941). This event, commonly termed as the drought of the 1950s, affected a large extent of the conterminous U.S. and is the most severe drought on record for the watershed. It coincides with the cold phases of both ENSO and PDO. ENSO actually oscillated mostly between La Niña and neutral conditions between May 1942 and February 1957 (Figure 3), the longest period in which the index remained in these phases. PDO shifted into its cold phase in November 1947 and remained mainly in this phase for up to February 1957. Another significant period of rainfall deficit started in 1962 and lasted up to 1965. It is associated with a drought that affected most of the northeast U.S. [*Namias*, 1966, 1967] and coincides with cold PDO and mostly neutral ENSO with La Niña conditions between May 1964 and February 1965.

[45] The 1976–1988 and 1991–1994 periods were that of normal and above normal precipitation across the watershed, with a few dry patches. Meteorological conditions prevailing were influenced by warm PDO (which started in July 1976) reinforcing multiyear El Niños (see Table 1). Year 1989, however, was a dry year across the whole basin, sandwiched between two wet periods. This lack of precipitation was influenced by negative ENSO (1988–1989 La Niña) and a weak PDO oscillating mostly between ± 0.5°C. Given that the 1988–1989 La Niña is one of the strongest (see Table 2), and is not reinforced (dampened) by a negative (positive) PDO, its influence on water availability is worth investigating further.

[46] The 2002–2004 drought is the second longest and most severe the region has experienced in recent record. It started earlier in the lower central arid portion and then propagated across the basin. Interestingly, this event did not coincide with La Niña conditions, but rather with neutral ENSO shifting into El Niño conditions, while PDO was in its cold phase until mid-2002 and shifted into its warm phase thereafter. Such dry conditions are not uncommon in the southwest as neutral ENSO with cold PDO can result in nearly as dry conditions as La Niña with cold PDO [*Goodrich*, 2004; *Quiring and Goodrich*, 2008]. The impact of such combination of the two indices on water availability will be further examined.

5.2. Climate Teleconnection With Precipitation

[47] Precipitation is the main determinant of water availability. To assess the relationship and spatial influence of climate variability on the precipitation in RG, climate indices were correlated with the average seasonal precipitation for each rainfall station. Kriging plots [*Delhomme*, 1978] for correlations with PDO (Figure 7), and ENSO indices (Figure 8) were constructed for winter (DJF), spring (MAM), summer (JJA), and fall (SON). The Pearson correlation coefficient, ρ_{xy}, forms the basis of the statistical test of independence. The null hypothesis is that the seasonal average precipitation is iid normal random variable not dependent on the indices. The magnitude and sign of the correlation coefficient are thus indicative of the existence, strength, and nature of any association [*Redmond and Koch*, 1991]. The correlation significance (p-value) for each station was also computed and is given (inset maps) along with the kriging plots. The p-value is the probability, if the test statistics is distributed as assumed in the null hypothesis, of observing a test statistic as extreme, or more, than the one

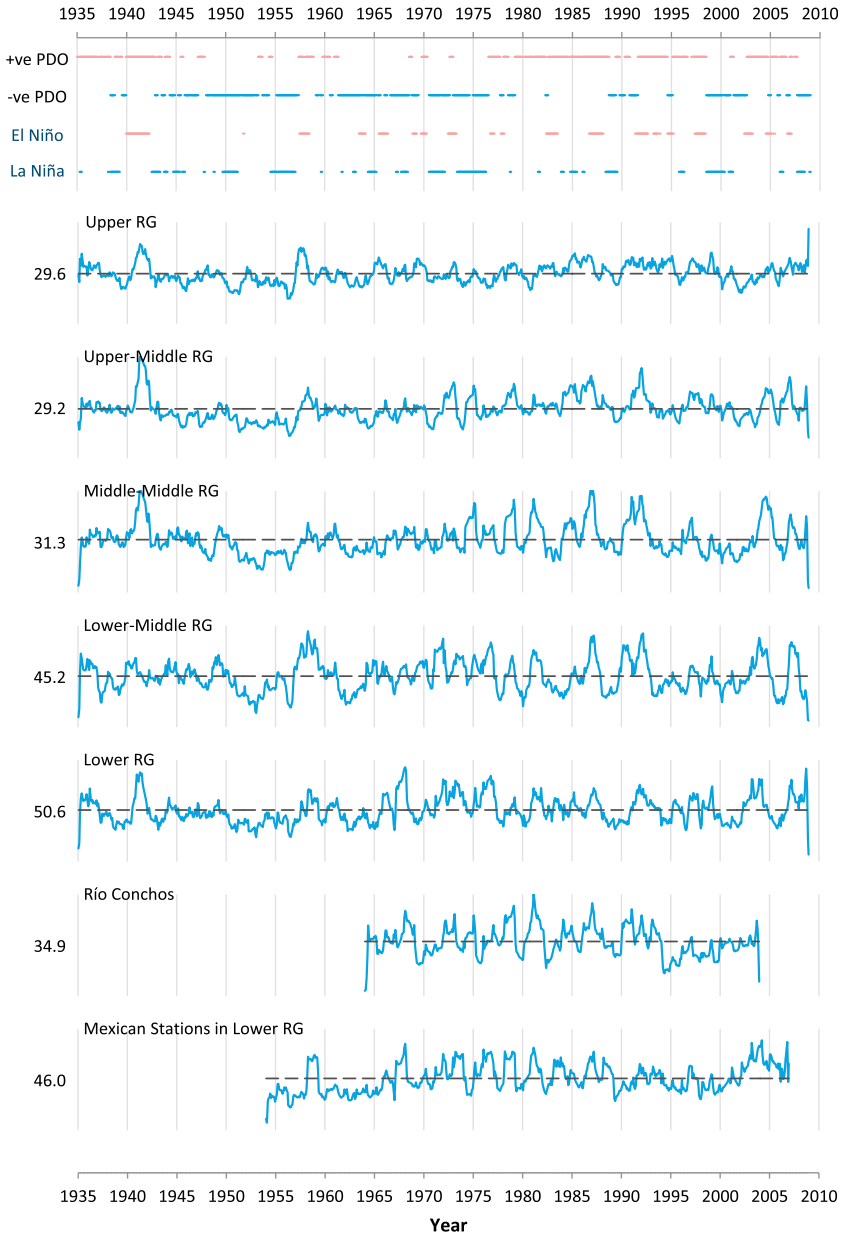

Figure 5. Smoothed series of average monthly gauged precipitation (mm/month) for each region. The broken horizontal line is the long-term average. The scales of the ordinates are arbitrary to illustrate variability. The top plot shows the phases of PDO and ENSO.

actually observed, i.e., how unlikely it may be due to chance. The *p*-values are stratified as follows: less than or equal to 0.01%, 0.1%, 1%, 1–5%, and greater than 5%.

5.2.1. PDO

[48] The PDO series between 1935 and 2008 has almost equal number of cold and warm years, thus prevents any bias that may result from the dominance of either phase over the other [*Kurtzman and Scanlon*, 2007]. The correlation structure is different for each season and varies considerably across the basin (Figure 7). The highest correlations are in winter and spring. In winter, a statistically significant positive correlation, ranging between 0.3 and 0.5, is observed in the lower RG region, especially in Mexico, at the mouth of the basin. This correlation structure shifts diametrically in the spring, with the northern semi-arid regions exhibiting higher correlation, while those in the lower half, from the Río Conchos downward, are statistically insignificant. The stations in the Río Conchos do not show any statistically significant correlation with PDO, except for one station in winter, at the mouth of this sub-basin. Summer precipitation, across the whole basin, exhibits no significant correlation with PDO, while negligible correlation is observed in some sections of the basin in the fall. Hence it is noted that despite relatively low correlation, PDO does have an influence on the winter and spring conditions in the southern and northern parts of the basin respectively. Therefore knowledge of the state of PDO is essential for water resources planning.

5.2.2. ENSO: Niño 3.4, MEI, and EMI

[49] The seasonal kriging plots for Niño 3.4 is given in Figure 8 and those for MEI and EMI are available as

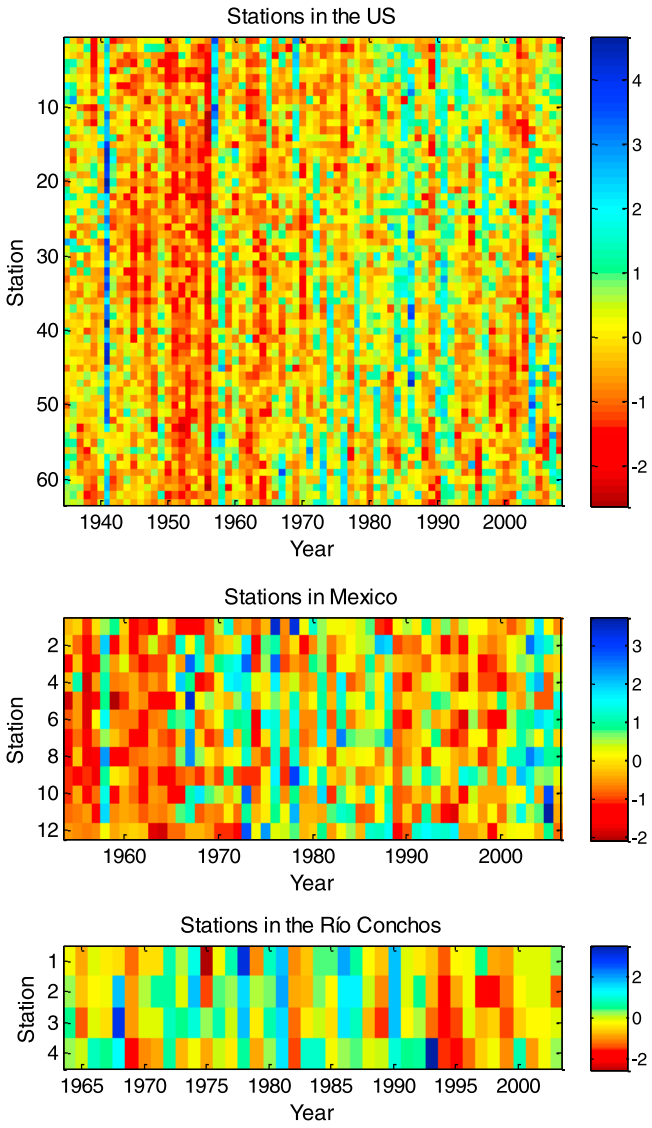

Figure 6. Time series of standardized anomaly for stations in the U.S., Mexico, and Río Conchos (stations are latitudinally arranged with numbers corresponding to Figure 2).

auxiliary material to this paper.[1] All three indices exhibit the same general seasonal correlation structure, but overall the correlation of EMI with precipitation is the weakest.

[50] Just like for PDO, the correlation structure is different for each season and varies across the basin. A positive, statistically significant correlation, ranging between 0.3 and 0.7, was observed for winter and spring across the whole basin, except for the Upper RG region which exhibits a negative correlation with ENSO. This negative correlation at the head of basin, in the Rockies, is consistent with the findings of *Smith and O'Brien* [2001] and *Patten et al.* [2003] on snowfall pattern in the United States. In spring, the highest correlation region is the Upper-Middle RG. From a water management perspective this finding is important as higher snowfall at the headwaters, during La Niña conditions, may offset reduced precipitation in New Mexico. In summer and fall, a negative correlation, even though not statistically significant, is observed, especially in the lower half of the basin.

[51] The correlation between EMI and precipitation is not statistically representative in the basin and may therefore not be useful for water management purposes. The correlation structures of Niño 3.4 and MEI are similar; therefore despite MEI's appeal as a more inclusive ENSO index, we shall adhere to NOAA's operational definition of El Niño and La Niña, as discussed in section 5.3.1 below, for the remainder of the paper.

5.3. ENSO Events

5.3.1. Definition of El Niño and La Niña

[52] The definition for El Niño has evolved over time; different investigations use different indices and criteria, thus producing dissimilar lists of events. For long, there was no specific definition for La Niña, despite an ongoing debate in the scientific community; they were defined in the context of the El Niño phenomenon [*O'Brien*, 2002]. *Trenberth* [1997] analyzed El Niño conditions between 1950 and 1997 using both Niño 3 and Niño 3.4 indices, relative to a base period climatology of 1950–1979, and suggested that an ENSO event is deemed to occur when the Niño 3.4 index is above (or below) ±0.4°C for at least six months. In 2003 the National Oceanic and Atmospheric Administration (NOAA) issued an official operational definition for El Niño and La Niña. The definition was endorsed by both Canada and Mexico in 2005 (North American countries reach

Table 1. El Niño and La Niña Events Between 1979 and 2008 Following NOAA's Definition

Begin	End	Duration
	El Niño Events	
May 1982	June 1983	14
September 1986	January 1988	17
May 1991	July 1992	15[a]
May 1993	July 1993	5[a]
October 1993	October 1993	1[a]
August 1994	February 1995	7[a]
May 1997	May 1998	13
May 2002	February 2003	10[b]
July 2004	January 2005	7[b]
May 2005	May 2005	1[b]
September 2006	January 2007	5
	La Niña Events	
July 1981	August 1981	2
November 1983	January 1984	3[c]
October 1984	May 1985	8[c]
January 1986	February 1986	2[c]
May 1988	June 1989	14
October 1995	March 1996	6
July 1998	April 2000	22[d]
October 2000	February 2001	5[d]
December 2005	March 2006	4
September 2007	May 2008	9

[a]Coupled El Niño event with a combined total of 28 months above +0.5°C.
[b]Coupled El Niño event with a combined total of 18 months above +0.5°C.
[c]Coupled La Niña event with a combined total of 13 months below −0.5°C.
[d]Coupled La Niña event with a combined total of 27 months below −0.5°C.

[1]Auxiliary materials are available in the HTML. doi:10.1029/2011JD016590.

Table 2. The Three Strongest ENSO Events Since 1979 Based on Different Criteria

Criteria	El Niño Event	La Niña Event
Duration above (or below) the defined threshold	1991–1995 2002–2005 1986–1988	1998–2001 1988–1989 1983–1986
Maximum (or minimum) temperature recorded	1982–1983 1997–1998 1986–1988	1988–1989 2007–2008 1998–2001
Total duration of event in the positive (or negative) phase	January 1990–July1995 April 2002–September 2005 June 1986–February 1988	June 1998–May 2001 August 1983–May 1986 April 1988–October 1989
ENSO intensity[a]	1997–1998 (1.325) 1982–1983 (1.068) 1986–1988 (0.759)	1988–1989 (−1.820) 2007–2008 (−1.715) 1998–2001 (−1.482)

[a]The numbers in parentheses are the intensities for associated events.

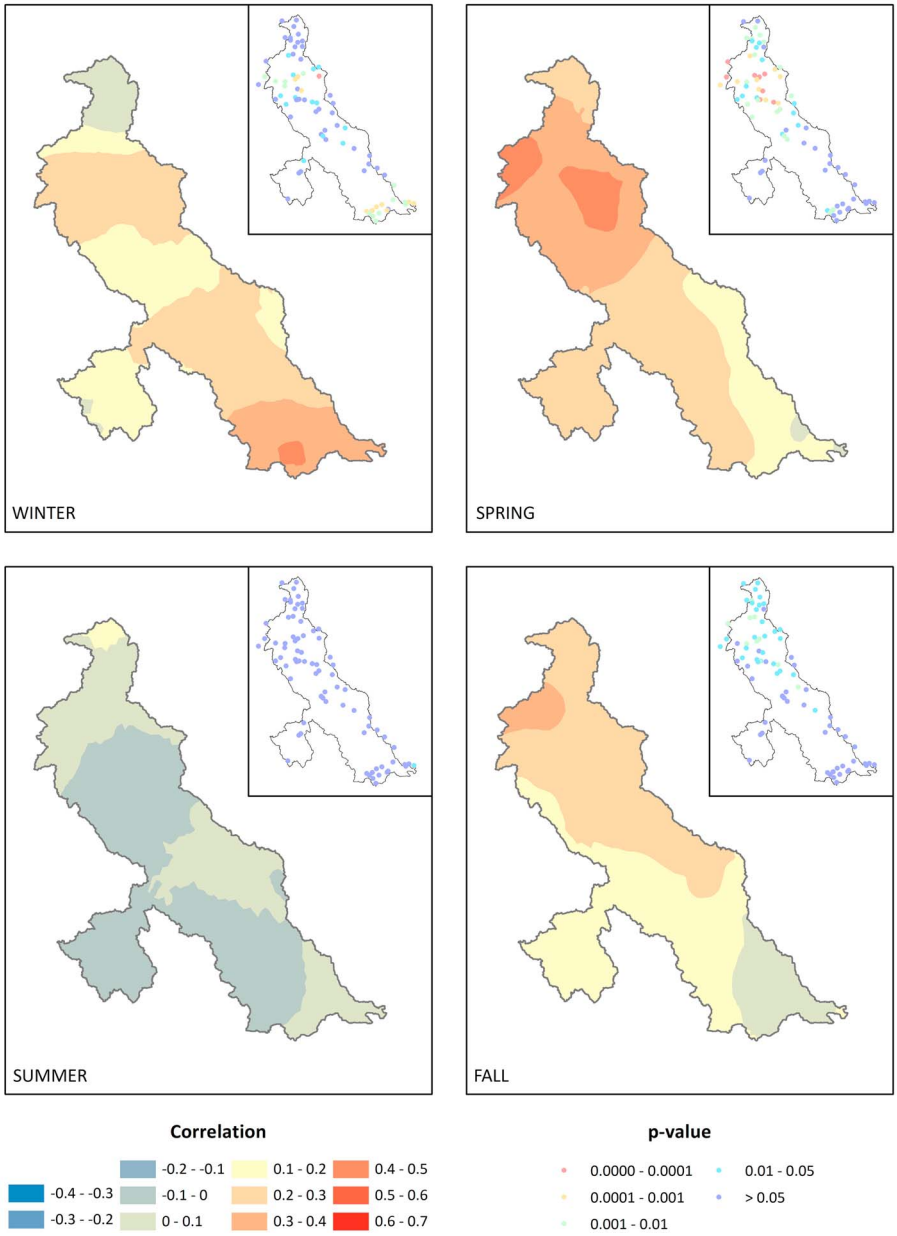

Figure 7. Plots of seasonal correlation coefficients between PDO and precipitation anomaly. Inset gives the p-values for the regression coefficients.

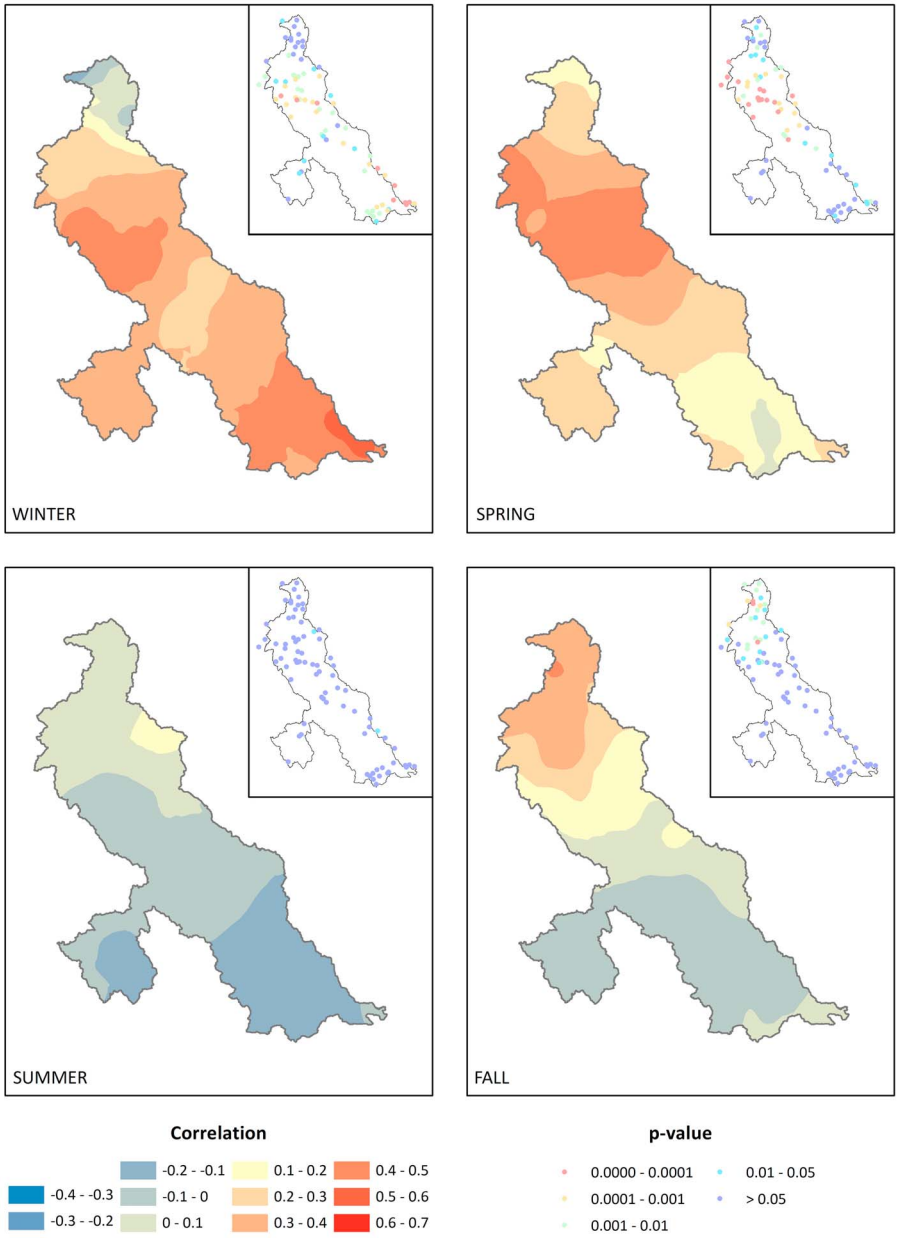

Figure 8. Plots of seasonal correlation coefficients between Niño 3.4 and precipitation anomaly. (Similar plots for MEI and EMI are available as auxiliary material.) Inset gives the p-values for the regression coefficients.

consensus on El Niño definition available at http://www.noaanews.noaa.gov/stories2005/s2394.htm) and has been adopted by the World Meteorological Organization Region IV [*Larkin and Harrison*, 2005]. Accordingly, an El Niño (La Niña) is defined as:

> A phenomenon in the equatorial Pacific Ocean characterized by a positive (negative) sea surface temperature departure from normal (for the 1971–2000 base period) in the Niño 3.4 region greater than or equal in magnitude to 0.5°C, averaged over three consecutive months.

[53] Neutral condition is when the index is between ±0.5°C. Figure 3 shows a plot of the Niño 3.4 index for 1935 to 2008, overlain with a centered 3-month moving average, which smoothens out variations in SST not associated with ENSO, and the ±0.5°C thresholds. The base period climatology for the IRI data set is 1951–1980 [*Kaplan et al.*, 1998] and was adjusted to 1971–2000 to satisfy the above definition. During that period, El Niño occurred 21% of the time and La Niña 27% of the time, i.e., the Pacific was either active in one of the two conditions or neutral about half the time.

5.3.2. Comparison of ENSO Events (1979–2008)

[54] Table 1 gives the start, end, and duration of El Niño and La Niña events occurring since 1979. The subscripts indicate coupled events where the average SSTA remained in one phase. NOAA's definition, unlike *Trenberth*'s [1997], does not specify a minimum period over which the average index has to be above (or below) the threshold to be deemed

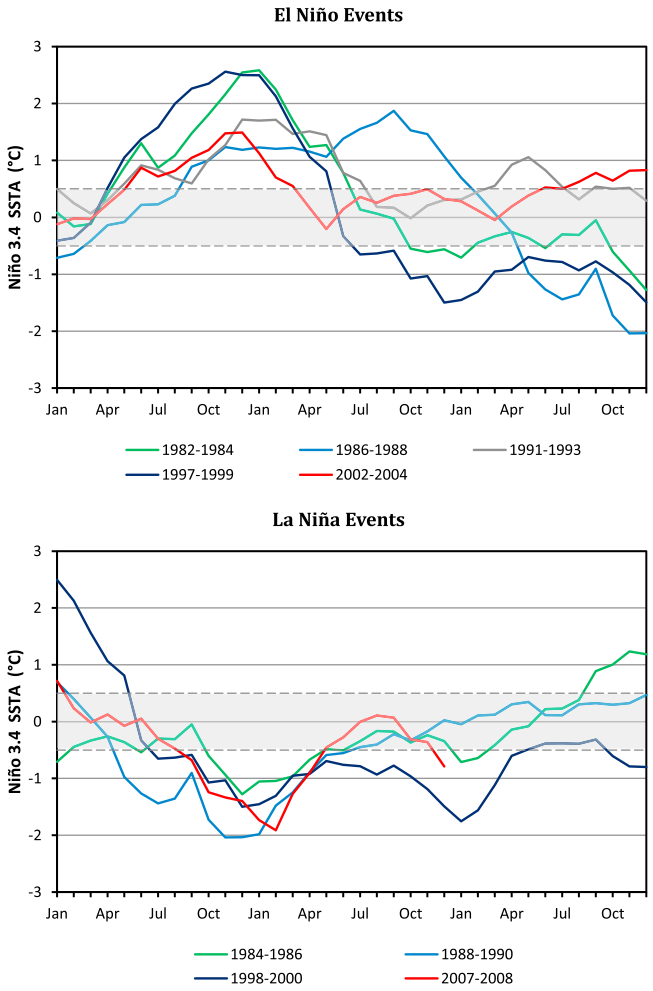

Figure 9. Comparison of major El Niño and La Niña events between 1979 and 2008 (transparent gray band shows ±0.5°C neutral range).

a significant event, thus smaller periods of one to three months are also included in the list. We note that between 1979 and 2008, El Niños generally lasted longer than La Niñas, and there were more months above the +0.5°C threshold, resulting in El Niños 26.4% of the time, as opposed to 21.1% for La Niñas. A higher frequency of El Niños since 1976 has been associated with decadal changes in the climate in the Pacific Ocean accentuated by recent climatic changes [*Kumar et al.*, 1994; *Trenberth*, 1990]. The two often called major El Niños (1991–1995 and 2002–2005) and major La Niñas (1983–1986 and 1998–2001) occurred between 1979 and 2008.

[55] The onset of ENSO event is not consistent; El Niño events typically begin between May and September and La Niña events begin between July and October, except for the 1988 event which started earlier, in May, and the 2005 event evolved later, in December. The time interval between El Niño events ranged between 15 and 47 months with an average of 33 months when coupled events are counted as one. In the case of La Niña events, the interval was normally around 26 months, except when the two major El Niño events occurred, leading to a gap of 75 and 57 months respectively. The time interval between phase shifts varies from as short as one month (1997–1998 El Niño to 1998–2001 La Niña) to neutral conditions lingering for up to 23 months (1988–1989 La Niña to 1991–1995 El Niño).

[56] Not all El Niños (La Niñas) are created equal; some events last for only a few months while others may persist for two or more calendar years. Figure 9 compares the recent strongest El Niño and La Niña events. El Niños (La Niñas) tend to peak (trough) between November and February, except for the 1986–1988 event which peaked earlier in September. The strongest El Niño has a higher Niño 3.4 index value compared to the lowest index value for the strongest La Niña. Two El Niños with maximum SSTA above +2°C were noted while La Niñas' maxima were within −1 and −2°C. The reason for this lies mainly in the depth of the thermocline, which is shallower on the easternmost part of the Pacific basin, and it is therefore harder for the cold tongue to get colder, thus explaining why El Niños tend to be stronger than La Niñas [*Neelin*, 2010].

[57] All these differences make it difficult to rank El Niños (La Niñas). It is hard to define the criteria to be used for such ranking; should it be (1) the duration above (or below) the defined threshold, (2) the maximum (or minimum) SST recorded, or (3) the total duration of the event in the phase of interest [*Wolter and Timlin*, 1998]? M. Glantz (The El Niño Olympics, or the Search for the El Niño of the Century, 1998, from Fragilecologies blog, http://fragilecologies.com/blog/?p=226) argues that a number of socio economic criteria, such as global spread of impacts, costs of devastation, or even public perception and media coverage, should also be considered. These criteria, however, are too complex and not totally objective and will thus not be considered in this study. Table 2 ranks the three strongest ENSO events, using the Niño 3.4 index, following *Wolter and Timlin* [1998], and intensity – a new metric which incorporates both SSTA and duration. ENSO intensity is the sum of monthly indices above (or below) the ±0.5°C threshold divided by the corresponding number of months. For combined events, the months where the index is within the neutral range are excluded.

5.3.2.1. Duration and Maximum/Minimum SSTA

[58] The ranking reveals some interesting results regarding the individuality of ENSO events. In both El Niños and La Niñas, the list of the three strongest events using duration above the threshold is very different from that using the maximum (or minimum) SSTA, implying that events persisting for long periods do not necessarily exhibit large deviations from the mean. The 1991–1995 event, for example, started in January 1990 and persisted until July 1995 [*Trenberth and Hoar*, 1996], and is the longest El Niño on record, with a combined total of 28 months above the +0.5°C threshold, but does not show up within the list of events with maximum temperature or intensity. *Allan and D'Arrigo* [1999], examining palaeoclimatic records of ENSO infer that such events are not unusual. El Niños persisting for three years or longer may occur around four to five times per century. On the other hand, instrumental records analyzed by *Trenberth and Hoar* [1996] indicate that this event is unlikely the result of natural decadal-timescale variation but is rather influenced by global warming. The 1997–1998 El Niño, which developed earlier than the scientific community expected, is also noteworthy and has been dubbed "the climate event of the century" [*Changnon and Bell*, 2000].

Unlike the 1991–1995 event, it lasted only 13 months but was still one of the strongest on record with a peak SSTA of 2.56°C, closely rivaling the 1982–1983 event [*Kiladis and Diaz*, 1986]. By contrast the 1990–1995 event had a peak temperature of only 1.71°C occurring within the first third of the event. This super El Niño, just like the one in 1982–1983, had a dramatic impact on global weather variability causing the second worst drought in Australia and devastating floods across the western United States, with record precipitation in California. Western Pacific Islands, Central America and Mexico experienced severe droughts. It ended abruptly in the middle of 1998 when a mass of cold water under-rode the warm surface waters causing one of the longest and strongest La Niña ever recorded.

[59] The 1998–2001 La Niña started in June 1998 and lingered till May 2001, with a combined total of 27 months below the −0.5°C threshold. The SSTA reached a minimum of −1.50°C in December 1998 and appeared to decay thereafter but resurged with a lower SSTA of −1.76°C in January 2000. The 1988–1989 La Niña, the second longest since 1979, reached a lower SSTA of −2.03°C in November 1988, and is one of the lowest on record.

[60] When the total duration the index remain in the positive or negative phase is considered, the same El Niños are ranked, but a slight difference is noted in the order of La Niñas. The 1983–1986 event, even though has fewer months below the threshold, takes longer to decay, and hence supersedes the 1988–1989 event.

5.3.2.2. ENSO Intensity

[61] ENSO intensity shuffles the ranking of El Niños based on maximum SSTA recorded. The 1997–1998 event, with an intensity of 1.325, surpasses the 1982–1983 event, even though the latter has the highest temperature among recent episodes. In the case of La Niña, the list based on intensity agrees with that based on temperature, but not with the one based on duration. The 2007–2008 La Niña, being a short event, does not feature in the list based on duration but has the second lowest temperature and intensity. It is also important to note that La Niñas have much higher intensities than El Niños as they generally have shorter durations.

[62] The effect of ENSO on water availability, based on the criteria discussed above, will be examined to ascertain if SSTA, duration, or intensity have different impacts. Note that in subsequent sections, ENSO events will be referred to as labeled in the legend of Figure 9.

5.4. Runoff and Water Availability

[63] Noah or LIS does not have a routing scheme; runoff is generated at 1/8° pixel level. Further, since the basin is divided into sub-regions rather than sub-basins, and because RG has a number of endorheic sub-basins, area-averaged runoff (AAR) is a better representation of regional water availability [*Shukla and Wood*, 2008].

$$AAR = \frac{\sum_{i=1}^{n} r_i}{\sum_{i=1}^{n} a_i} \tag{2}$$

where r is the pixel runoff at the temporal scale of interest, a is the area of the corresponding pixel, and n is the number of pixel in the sub-region considered.

[64] Before assessing changes in water availability, we evaluated NLDAS-2 and runoff from Noah LSM against observations to assess the validity of our approach.

5.4.1. Model Validation

5.4.1.1. Precipitation

[65] The precipitation field in NLDAS-2 is derived from a number of sources whose coverage near the U.S. borders and beyond is often limited. The product has been extensively validated over CONUS but has not received the same treatment beyond the U.S. borders. Given that RG is a transboundary basin, extending into Mexico, and that the density and length of precipitation record in Mexico is low, it is important to verify the adequacy of NLDAS-2 over the Mexican portion of the basin. We selected three of the six sub-regions within the basin, one in the U.S. and two in Mexico, for validation. The Upper-Middle RG has a dense rain gauge network, with 31 stations; it is found almost entirely within the state of New Mexico and therefore benefits from the high quality products used in generating NLDAS-2. The two regions in Mexico are the Río Conchos and the Lower RG. Río Conchos, located entirely within Mexico, is an important sub-basin, but has only four viable stations aligned along the major axis of the catchment. The major portion of Lower RG is located within Mexico, and has 5 stations along the U.S. border and 11 stations in Mexico. We therefore compared the NLDAS-2 precipitation field with the observations from the Mexican stations.

[66] The precipitation field in NLDAS does not agree very well with station observations at the hourly timescale, but as the data is aggregated over longer timescales the correlation increases [*Luo et al.*, 2003]. This is because NLDAS-2 precipitation is generated from multiple sources and averaged over the domain of interest. We compared precipitation at the monthly scale. Figure 10 shows the scatterplots of the area-averaged monthly precipitation (similar to AAR) derived from the NLDAS-2 precipitation field (M) against average monthly observed precipitation from gauges (O) within each sub-region. The data length differs, as shown by the total number of data points (N) in each plot. The relative bias, root mean square deviation (RMSD), and correlation coefficient (ρ) are given for each region, along with the identity (1:1) line.

$$Relative\ \ Bias = \frac{\overline{M} - \overline{O}}{\overline{O}} \tag{3}$$

$$RMSD = \sqrt{\frac{\sum_{i=1}^{N} (M_i - O_i)^2}{N}} \tag{4}$$

[67] All three regions have very high ρ values implying that the precipitation field in NLDAS-2, at the monthly timescale, over the entire RG basin is in good agreement with observations. A small consistent bias is noted toward observations, similar to the findings reported by *Luo et al.* [2003]. The RMSD values for the Río Conchos and Lower RG are greater than that for the Upper-Middle RG by a factor of three. This can be attributed to the fact that the Upper-Middle RG has a dense network uniformly spread over the whole region, while in Mexico the density and spread is limited. Also, most stations in Mexico did not have

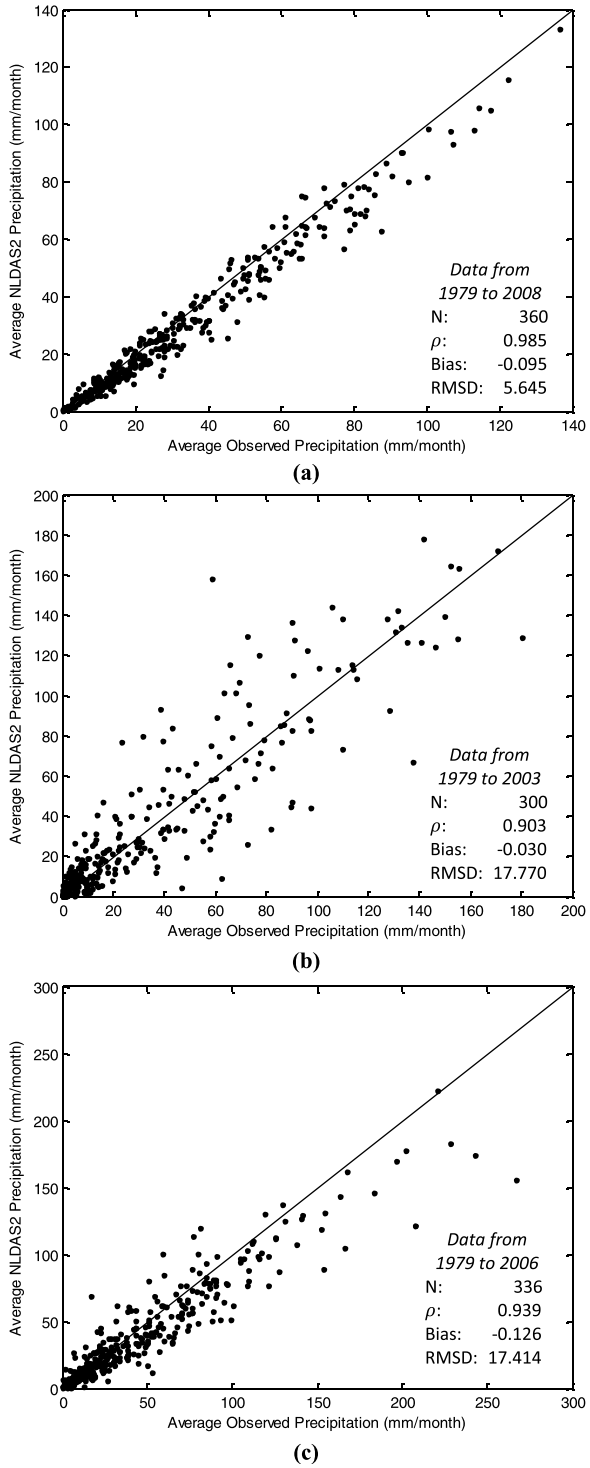

Figure 10. Scatterplot of area-averaged monthly NLDAS-2 precipitation and observed precipitation for the (a) Upper-Middle RG, (b) Río Conchos, and (c) Lower RG region (Mexican stations only).

a continuous series but have been reconstructed from observations available from adjoining sites.

5.4.1.2. Runoff

[68] In order to assess the representativeness of the modeled runoff we compared AAR of the Río Conchos, which is a closed sub-basin, unlike the other sub-regions, to measured values at Ojinaga, which is located at the confluence of the Río Conchos with RG. Historical mean daily discharge data for RG at Ojinaga is available from the International Boundary and Water Commission (IBWC) (http://www.ibwc.state.gov/). This data set, as can be expected, incorporates land-use-land-cover changes, the effect of dams, diversions, and other infrastructural changes. A data set of naturalized monthly flow, extending up to 2000, for the Río Conchos at Ojinaga is also available [*Sandoval-Solis et al.*, 2010]. The naturalization process utilized streamflow recorded at gaging stations and adjusted to remove the effect of reservoir storage and evaporation, water supply diversions, and return flows from surface and groundwater, so that the resulting series is as close to flow unimpaired by engineering infrastructures. However, the influence of land-use-land-cover changes, infiltration, surface storage-flow, subsurface storage-flow, and evapotranspiration cannot be adequately accounted for [*Wurbs*, 2006]. Noah accounts for evaporation, infiltration, and other hydrological parameters; but land-use-land-cover was kept constant to minimize extraneous noise that may interfere with the climate teleconnection signals. Figure 11a gives the plot of AAR, naturalized, and observed time series of monthly streamflow in the Río Conchos. Prior to any inference, it is important to point out that none of these three series are accurate representation of flow in the basin; each have different intrinsic limitations. Figure 11b gives a 12-month-sliding-window correlation plot for the period January 1998 to December 2000, which includes the period for which Noah was validated by *Lohmann et al.* [2004], thereby giving a benchmark for comparison. Each value in the graph is the Pearson correlation coefficient for 12 consecutive months starting from the month at which it is plotted. This process allows us to compare the consistency in the correlation across different seasons.

[69] It can be noted that Noah faithfully captures the monthly variations in runoff in the basin. Surprisingly, however, the correlation between AAR and the measured flow is consistently higher than with naturalized flow. This may be a function of the naturalization procedure, where evapotranspiration and other hydrologic processes cannot be amply determined given their complexity. Another notable feature of the running correlation is the periodic variation in the correlation values. The correlation is generally between 0.85 and 0.95 except for certain short intervals, which may be attributed to reservoir operation and diversions affecting the recorded flow. *Lohmann et al.* [2004] reported a correlation of 0.954 for the Nehalem River in Oregon which is a much smaller watershed (1,727 km^2) compared to the Río Conchos (64,000 km^2). In the larger snow dominated Wind River in Wyoming (4,897 km^2), a very low correlation of 0.117 was obtained which was due to a difference in the timing of snowmelt in Noah. The highest correlation across the series is generally noted in the fall and winter, and this can be explained by multiple factors: the timing of snowmelt [*Pan et al.*, 2003; *Sheffield et al.*, 2003], the influence of the NAM [*Hogue et al.*, 2005], and the influence of engineering infrastructures, such as dams, return flows, and unmetered diversions for agricultural purposes within the basin. Given that summer and early fall are the wettest months for the region (Figure 4), streamflow may initially stored in the reservoirs and any excess thereafter is released once the

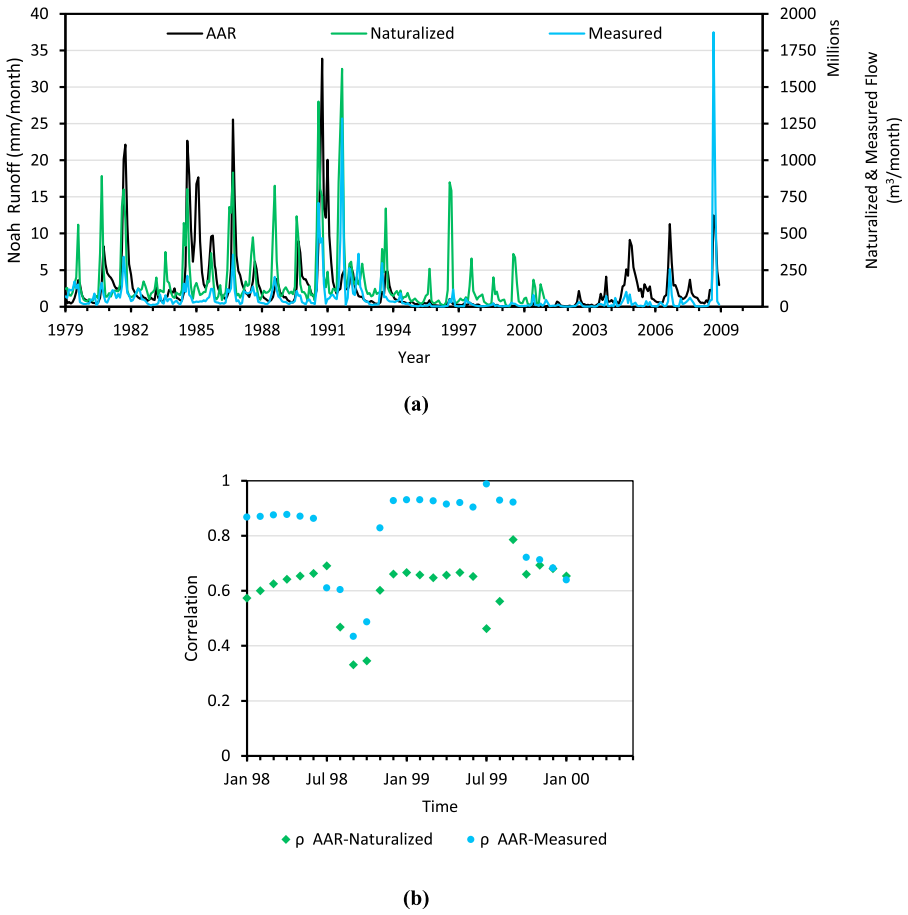

Figure 11. (a) Modeled, naturalized, and measured streamflow in the Río Conchos sub-basin. (b) Sliding-window correlation.

reservoirs have reached capacity and hence recorded at the downstream stream gauge as values closest to the natural variations.

5.4.2. Temporal Patterns of Climate Indices, Precipitation, and Water Availability

[70] Continuous wavelet transform allows the study of the temporal structure of precipitation and runoff across the basin and make inferences on the influence of climate variability patterns. The continuous wavelet power spectrum of AAR from each section of the basin is given in Figure 12b and can be compared against those of the four climate indices considered in this study (Figure 12a). The time spans for the plots of climate indices are the same as for runoff, i.e., 1979 to 2008. We used the MATLAB® based software package developed by *Grinsted et al.* [2004] (available from http://www.pol.ac.uk/home/research/waveletcoherence/) for generating the wavelet plots. The statistical significance of the peaks in the wavelet spectrum was tested using Monte Carlo methods against a lag-1 autoregressive red noise background; peaks with greater than 95% confidence are designated by thick black contours in the figures. However, regions out of these 95% confidence level areas should not be construed as the product of noise only. Natural processes are also present in these regions, albeit having a lower bearing on the power spectrum, and information on the influence of climate teleconnections can still be garnered from them [*Anctil and Coulibaly*, 2004].

[71] PDO has a cycle of about 20 to 30 years, which is not apparent in this wavelet power spectrum, as it is limited to 1979 to 2008 only. During this time span, the index was mostly positive until 1995 after which it oscillated with a period of three and a half years in each phase (Figure 3). This cycle is visible in the continuous wavelet power spectrum. ENSO has a much shorter wavelength, with a recurrence pattern of 3 to 6 years and every event normally lasts for around a year. Significant power in this band is observed throughout the entire record in the wavelet power spectrum of both Niño 3.4 and MEI, along with weaker significant power in the 1.5 to 2 year band associated with secondary variations in the indices while in a particular phase. Niño 3.4 and MEI have very similar power spectrum as they are highly correlated (ρ = 0.92). The plot for EMI is different from the latter indices as it has a different mode and evolves with a different frequency [*Ashok et al.*, 2007].

[72] Variations at both ENSO and PDO frequencies are apparent in the wavelet power spectrum of AAR. Significant powers in the smaller period (higher frequency) band are the result of seasonal variations. It is worth pointing that the continuous wavelet power spectra of both the averaged gauged precipitation and the first principal component of gauged precipitation for each sub-region (not shown here) exhibited variations similar to ENSO and PDO frequencies, further supporting the correlations established in section 5.2.

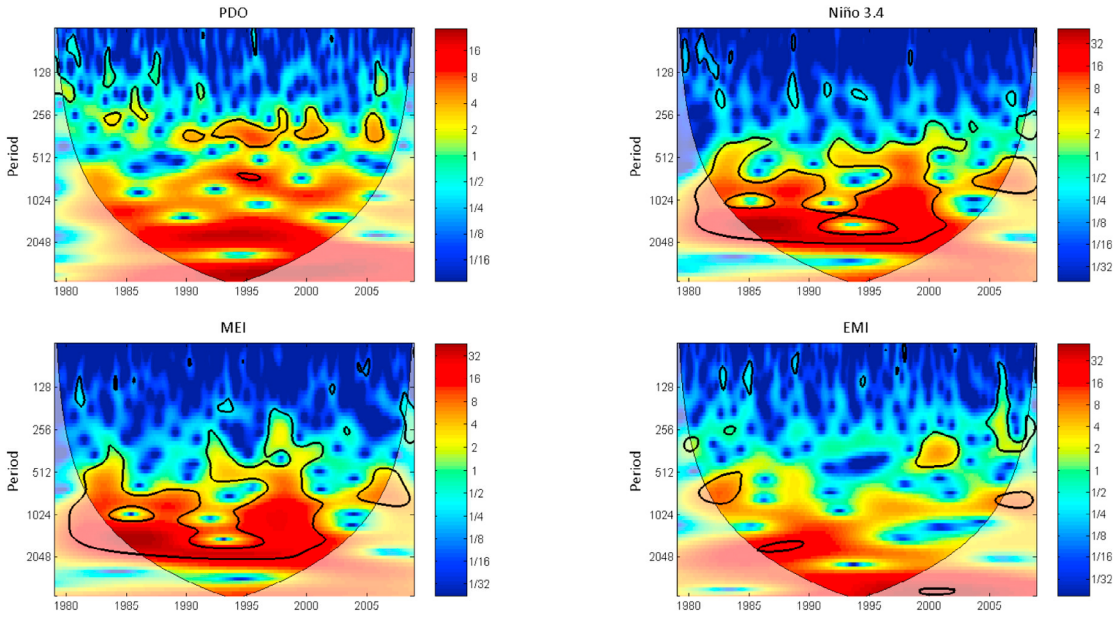

(a)

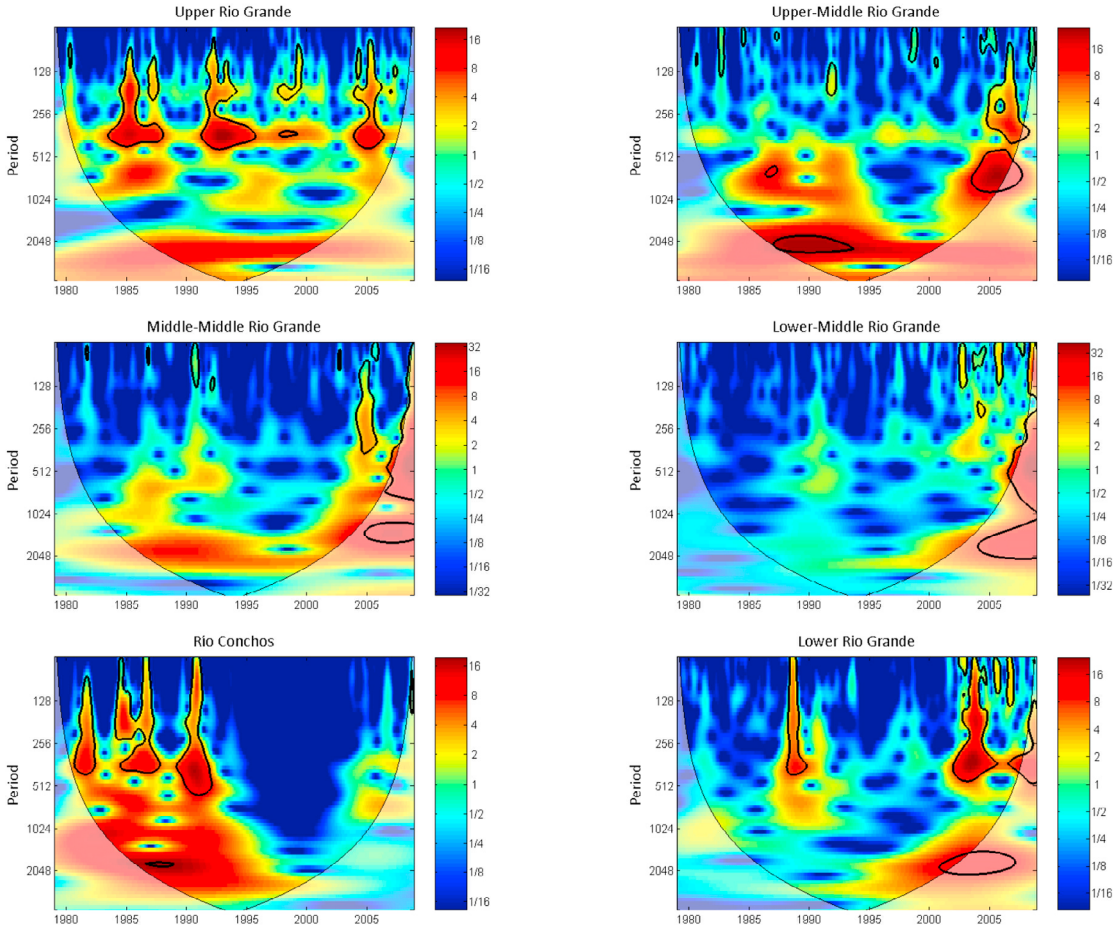

(b)

Figure 12. Continuous wavelet power spectrum of (a) climate indices and (b) AAR for each region. Period is in days. The thick black contours designate the 5% significance level against red noise and the thin black line demarcate the cone of influence beyond which, shown in a lighter shade, the image may be distorted since the data is not padded at the edges.

Table 3. Lag Correlation of Niño 3.4 Index With Noah Runoff for the Whole of the Basin[a]

	El Niño Event					La Niña Event			
Lag (Months)	1982–1984	1986–1988	1991–1993	1997–1999	2002–2004	1984–1986	1988–1990	1998–2000	2007–2008
−6	0.332	0.464	−0.375	**0.659**	−0.409	−0.004	−0.047	**−0.790**	−0.319
−5	0.237	**0.555**	−0.276	**0.542**	−0.073	−0.175	−0.217	**−0.681**	−0.322
−4	0.120	**0.628**	−0.182	0.432	0.193	−0.261	−0.453	−0.428	−0.202
−3	−0.144	**0.669**	−0.091	0.332	0.351	−0.323	−0.539	−0.102	−0.056
−2	−0.272	**0.668**	0.051	0.272	**0.551**	−0.324	−0.508	0.299	0.058
−1	−0.226	**0.627**	0.283	0.102	**0.562**	−0.228	−0.415	0.426	0.329
0	−0.350	**0.562**	**0.597**	−0.185	0.456	−0.300	−0.102	0.354	**0.649**
+1	**−0.509**	0.293	**0.707**	−0.370	0.210	−0.355	−0.086	0.311	**0.675**
+2	−0.384	0.085	**0.730**	**−0.485**	−0.094	**−0.471**	−0.077	0.251	**0.614**
+3	0.031	−0.093	**0.622**	−0.453	−0.187	−0.339	0.069	0.121	0.450
+4	0.002	−0.223	0.405	−0.287	−0.242	−0.074	0.266	−0.021	0.178
+5	−0.019	−0.294	0.151	−0.289	−0.145	0.180	**0.511**	−0.054	−0.148
+6	−0.025	−0.322	−0.040	−0.262	−0.276	0.213	**0.649**	0.010	−0.431

[a]Boldface values are statistically significant at $p < 0.05$.

The fact that the influence of climate variability was more apparent in precipitation than in streamflow is because runoff is not a first order response of precipitation but is filtered by the watershed characteristics [*Legates et al.*, 2005]. Looking closer at each spectrum we note that in the Upper RG region significant power at the 5% significance level is exhibited within the high frequency band, coincident with the pattern exhibited by the PDO spectrum but ENSO related patterns were not significant at the 5% level. In the Upper-Middle RG region, however, variations at the ENSO frequencies are clearly evident in most part of the spectrum except for the period 1995 to 2003. In the Middle-Middle RG region, the spectrum exhibited variations in the ENSO frequencies even though not statistically significant throughout. The spectrum for the Lower-Middle RG region was devoid of statistically significant powers as can be expected, because the correlation of ENSO indices with precipitation is consistently lower than in its two adjoining regions (Figure 8). In the Lower RG region variations at ENSO frequencies is visible in the second half of the series. It should be noted that this region is close to the Gulf of Mexico and subject to oceanic influences and hurricanes whose effects are embedded in the model outputs. In the Río Conchos, variations at ENSO frequencies are evident in the first half of the series but completely absent in the second part when the basin was subjected to an exceptional drought.

5.5. Effects of Large-Scale Climate Indices on Water Availability

[73] After having established the spatial correlation of precipitation with large scale climate indices and investigated the sensitivity of runoff to PDO and ENSO using continuous wavelet transform, we now discuss the changes in water availability with respect to major El Niño and La Niña events. We also determine if there is any lag in runoff relative to ENSO.

5.5.1. Lag Correlation

[74] To investigate the lag between individual ENSO events and runoff in RG we considered an 18 months long series encompassing each event. Most events peaked in early winter; therefore the series considered extended from March before to August after the peak. The 1986–1988 El Niño peaked earlier in September and thus the range considered was from December before to May after the peak. Table 3 gives monthly lag correlation coefficients of AAR of the whole RG basin relative to the Niño 3.4 index. The lag is defined by the month having maximum statistically significant correlation. A positive lag indicates that the index led runoff. Lags ranging between 0 to 3 months were observed for AAR of the whole basin with respect to most El Niños and La Niñas. It is interesting to note that for some events a negative correlation was observed despite the fact that there is an overall dominant positive correlation between ENSO and runoff in the basin.

[75] Lag correlation was also computed for each subregion and the consolidated result of the statistically significant correlations is shown in Figure 13. For the 1998–2000 La Niña, which is bimodal, the lags shown are with respect to the second dip as it has a lower SSTA. In the Upper RG the lag is 3 to 4 months. In the Middle-Middle RG a consistent lag of 1 to 4 months is observed relative to most El Niño events and in the Río Conchos a lag of 0 to 5 months is observed relative to three of the four La Niñas considered. This result is consistent with the findings of *Chen and Kumar* [2002] who used a large-area basin-scale LSM to investigate the relationship among terrestrial hydrologic processes with ENSO over North America and *Kumar and Hoerling* [2003], who compared and confirmed the observed lag in zonal mean tropical thermal anomalies with respect to east Pacific SST using an atmospheric GCM.

5.5.2. Changes in Water Availability

[76] In order to assess the effects of ENSO events on water availability, the seasonal percentage change with respect to the long-term average in AAR, for each sub-region and for the whole basin was computed (Figure 14). ENSO events typically peak around November and since the lag between ENSO and runoff was found to be generally between 0 month to a season, water availability in winter and spring are expected to be most influenced. Note, however, that the 1986–1988 El Niño and 1998–2000 La Niña do not fit the general trend. The 1986–1988 El Niño lingered for a year before reaching its peak temperature and the 1998–2000 La Niña was bi-modal, with two distinct troughs, over a 27-month period.

[77] The first thing we note is that even though there is a general tendency for an increase (decrease) in runoff during El Niños (La Niñas), some events actually caused a decrease (increase) in water availability.

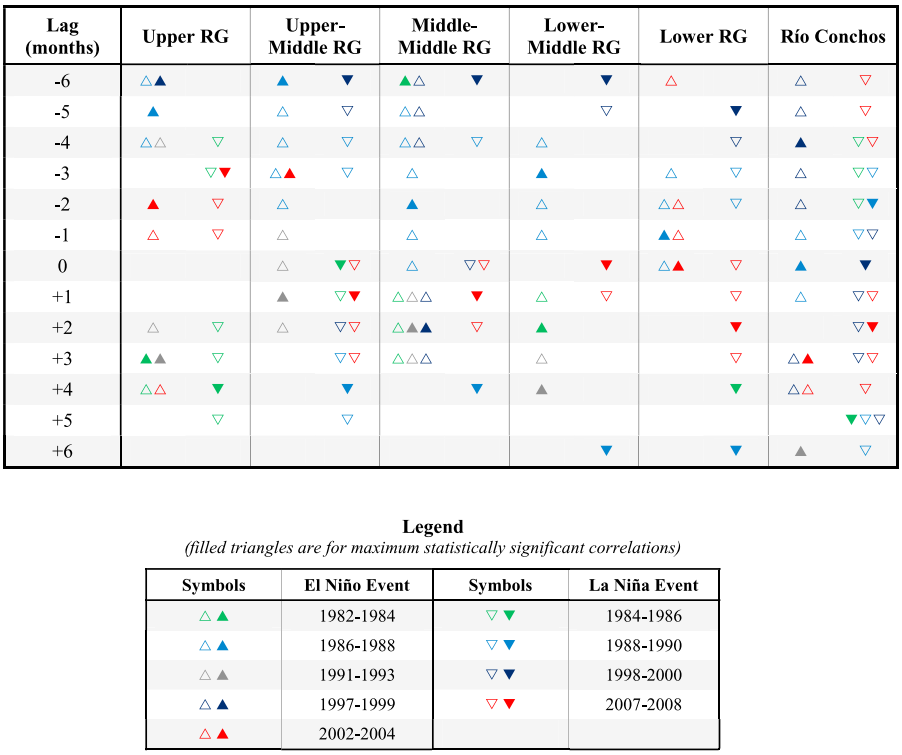

Figure 13. Lag correlation for each section of the basin.

[78] PDO generally enhances ENSO events [*Kurtzman and Scanlon*, 2007], therefore we also consider the phases of PDO for corresponding major El Niño and La Niña events in our discussion. Table 4 gives the coincident phases of PDO with respect to the ENSO events considered. We note that some El Niños (La Niñas) were strengthened by positive (negative) PDO, while others coincided with weak or transitioning PDO.

5.5.2.1. El Niño and PDO

[79] The 1986–1988 El Niño, even though was the third strongest event since 1979 (Table 2), brought the highest percentage increase in runoff for the whole basin (196%), with the upper half of the basin gaining between 190 to 350% more runoff in winter. The lower half, including Río Conchos experienced a more modest increase of around 60%. The same pattern, but with lower percentages, persisted in spring and summer. The event was enhanced by a strong positive PDO – both events evolved synchronously and peaked in August 1987 (Figure 3).

[80] The 1991–1993 El Niño coincided with a PDO transitioning into its positive phase. It triggered the same pattern in runoff but with slightly lower percentages (average of 147% for the whole basin). The Río Conchos benefited from the highest increase in runoff in spring during that event, compared to all other El Niños. This event had the longest duration above the ±0.5°C threshold among the El Niños considered, but was not within the top three in terms of maximum temperature recorded. It had three peaks; the two following the first one, however, have lower SSTAs. The second peak coincided with positive PDO and the third one coincided with a temporary shift in the phase of PDO to negative. Interestingly, the percentage change in AAR was negative across the basin during both the second and third peaks.

[81] The 1982–1984, 1997–1999, and 2002–2004 El Niños did not generate higher runoff in the basin, but rather a decrease in water availability. AAR was lower by 50% over the whole basin and over 90% in the Río Conchos subbasin. The 1982–1984 and 1997–1999 events were two of the strongest El Niños on record, based on ENSO intensity and maximum temperature recorded. They both coincided with weak PDO; the 1982–1984 event starts when PDO was in its positive phase but peaked when the latter was almost neutral, oscillating between phases. The 1997–1999 event coincided with a PDO decaying from its positive to negative phase.

5.5.2.2. La Niña and PDO

[82] AAR in the basin was normally lower than the long-term average during La Niña winters and springs, except for the 1984–1986 event. The three events (1988–1990, 1998–2000, and 2007–2008) that caused a decrease in water availability occurred when PDO was either in its negative phase or transitioning from positive to negative. Given that the 1998–2000 event is the longest La Niña since 1979 (27 months) and is bimodal, with the second dip, occurring in January 2000, having a lower SSTA and coinciding with negative PDO, we also computed the change in water availability following the second dip (not shown in Figure 14). A decrease in AAR was noted across all subregions, except for winter in Upper RG (increase of 6%) which exhibits negative correlation with ENSO. The total decrease in AAR for the whole basin was nearly 60% for year 2000.

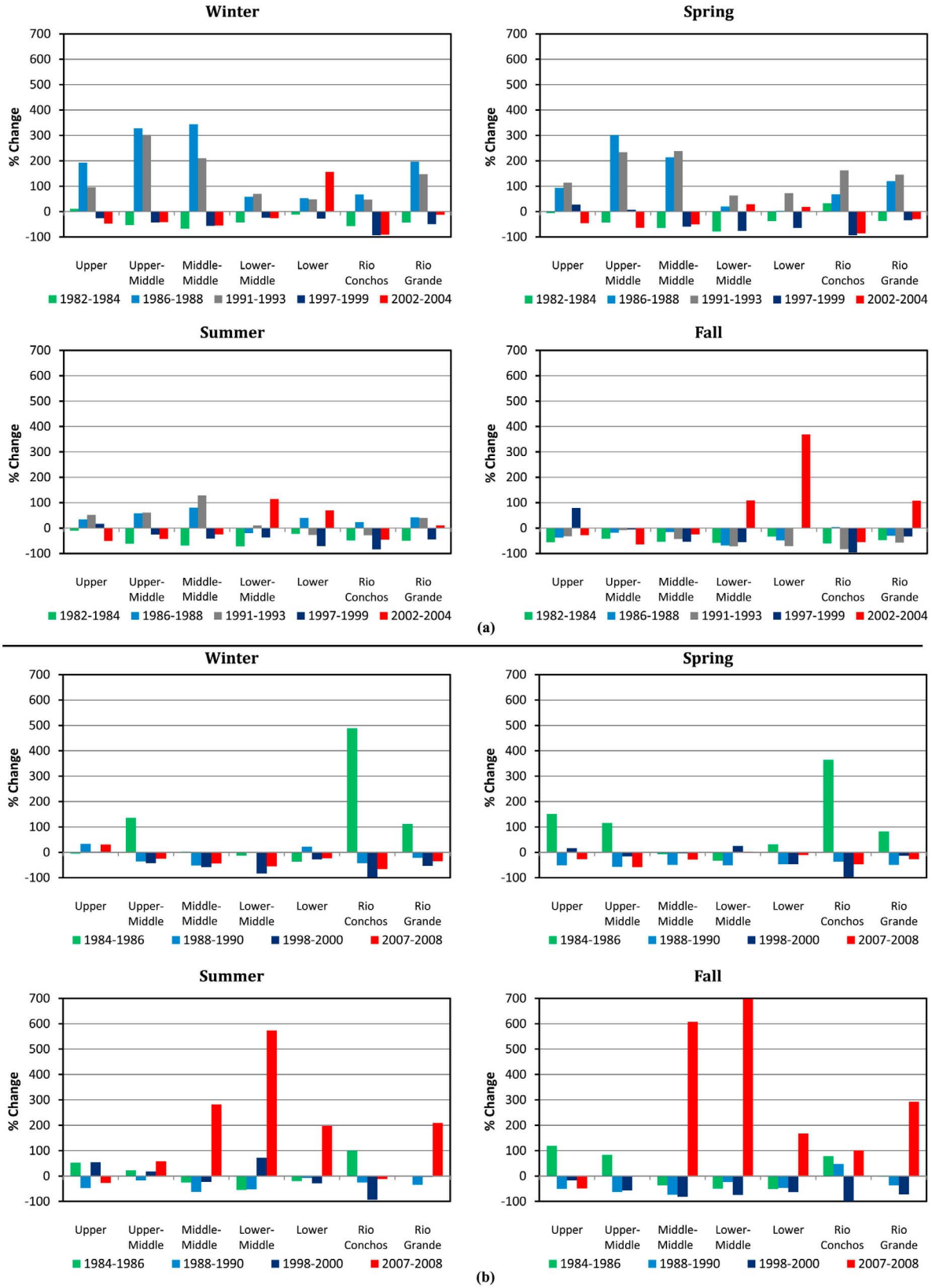

Figure 14. Percentage change in water availability during (a) El Niño and (b) La Niña events.

Table 4. PDO Phases for Major ENSO Events[a]

El Niño Event	PDO Phase	La Niña Event	PDO Phase
1982–1984	Weak but overall +	1984–1986	+
1986–1988	+	1988–1990	Transitioning (+ to −)
1991–1993	Transitioning (− to +)	1998–2000	Transitioning (+ to −)
1997–1999	Transitioning (+ to 1)	2007–2008	−
2002–2004	+		

[a]Symbols: +, positive; −, negative.

[83] The 1984–1986 La Niña coincided with a positive PDO and was the only event that caused an increase in water availability. An exceptionally large increase is noted in the Río Conchos in both winter and spring, which translated in an increase for the whole basin. These results are consistent with the analysis of multiyear droughts in the past three centuries by *Cole et al.* [2002] who showed that persistent negative PDO enhances the impact of La Niña related droughts, while oscillating PDO produced moderate and/or localized droughts, and a positive PDO would suppress drought despite persistent La Niña conditions.

[84] Based on the above observations, we note that PDO has an important influence on water availability in the basin. A positive PDO enhances the effect of El Niño and dampens the negative effect of La Niña. When PDO is in a neutral/transition phase, La Niña dominates climatic conditions and reduces water availability. El Niños lingering for long periods have more influence on water availability than short duration high intensity events. Finally it is interesting to note that the percentage increase during El Niños significantly offsets the drought-causing effect of La Niñas. This finding should not be discounted in long-term water resources planning.

6. Conclusions

[85] Local meteorological and hydrological variables, and hence water availability, are influenced by large-scale climate indices. In this study we investigated the influence of ENSO and PDO on the water availability in RG by first establishing the spatial and temporal variation of the correlation between climate indices and gauged precipitation across the basin and then determining percentage changes in water availability as derived from an LSM, instead of using streamflow which is constantly impacted by activities in the basin masking climate influences. The following conclusions are drawn from this study:

[86] 1. The correlation between PDO and three ENSO indices, namely Niño 3.4, MEI, and EMI, with gauged precipitation respectively shows that both ENSO and PDO have a strong influence on the winter and spring precipitation in the basin. The overall correlation is positive, except for the Upper RG section which includes the headwaters in the San Juan range in the Rocky Mountains in southern Colorado. Therefore, higher snowfall during La Niña conditions may help in maintaining flow in the river and offset precipitation reduction in arid/semi-arid New Mexico.

[87] 2. The correlation between the Niño 3.4 and MEI indices with precipitation are similar since they are closely related. The temporal structure and influence of EMI is different and is not strongly correlated with precipitation in the basin.

[88] 3. Additional information can be garnered by examining the major El Niño and La Niña events by classifying them using four criteria (duration above defined threshold, maximum or minimum SSTA, duration in phase of interest, and intensity). ENSO events are not equivalent, some events have short duration but high intensity, while others lingers for several years with lower SSTA.

[89] 4. Runoff across the basin was generated using the Noah LSM and AAR was used as a proxy for water availability. The basin was divided into six sub-regions for analysis purposes. Continuous wavelet power spectrum shows the extent of influence of ENSO and PDO on runoff. Variations at both ENSO and PDO frequencies are apparent in the wavelet power spectrum of AAR for each region.

[90] 5. The influence of individual ENSO events, five El Niños and four La Niñas between 1979 and 2008 and corresponding phases of PDO, on water availability in the basin was investigated. Lags ranging between 0 to 3 months were observed between runoff and ENSO events. A general increase (decrease) in runoff during El Niños (La Niñas) was noted but some individual events actually caused a decrease (increase) in water availability. El Niños lingering for long periods have more influence on water availability than short duration high intensity events. The upper-middle section of the basin records a higher increase in winter water availability during El Niño events (200–300%) while the lower half, including the Río Conchos, experiences a more modest change.

[91] 6. PDO has an important influence on water availability. A positive PDO enhances the effect of El Niño and dampens the negative effect of La Niña. When it is in its neutral/transition phase, La Niña dominates climatic conditions and reduces water availability.

[92] 7. The percentage increase during El Niños significantly offset the decrease registered during La Niñas. This finding is important for water resources planning.

[93] The study extends the discussion between the influence of large-scale circulation indices and local meteorological and hydrological conditions by quantifying the seasonal percentage changes in water availability, which is more tangible information for water planning. Climate change may alter the frequency and intensity of ENSO events and may cause droughts that are more extreme and/or of longer duration than on record. The current results, while are not intended for prediction purposes, may help in the long term sustainable water planning and management within the basin for both the United States and Mexico. Finally, the methodology adopted in this paper is not limited to the watershed scale but can be applied to larger continental scale to assess the need and effectiveness of interstate water transfers.

[94] **Acknowledgments.** The authors thank Brent D. McRoberts and John W. Nielsen-Gammon of the Department of Atmospheric Science at Texas A&M University for providing the precipitation data set for the U.S. and Rosario Sanchez and the Comisión Nacional del Agua for providing the data set for Mexico. Goddard Earth Sciences and Technology Center supported the first author's stay at NASA Goddard Space Flight Center, Greenbelt, Md. Thanks are due to the LIS software team, particularly Sujay Kumar and Jim Geiger, for their technical support. The authors are grateful to Sara C Pryor, the Editor, and three anonymous reviewers for their useful comments and suggestions. This research was

partially funded by the Comisión Estatal de Aguas y Saneamiento del Estado de Coahuila, Mexico through Texas AgriLIFE Research and USGS grant 2011TX395B.

References

Adams, D. K., and A. C. Comrie (1997), The North American monsoon, *Bull. Am. Meteorol. Soc.*, *78*(10), 2197–2213, doi:10.1175/1520-0477(1997)078<2197:TNAM>2.0.CO;2.

Allan, R. J., and R. D. D'Arrigo (1999), 'Persistent' ENSO sequences: How unusual was the 1990–1995 El Niño?, *Holocene*, *9*(1), 101–118, doi:10.1191/095968399669125102.

Anctil, F., and P. Coulibaly (2004), Wavelet Analysis of the interannual variability in southern Québec streamflow, *J. Clim.*, *17*(1), 163–173, doi:10.1175/1520-0442(2004)017<0163:WAOTIV>2.0.CO;2.

Ashok, K., S. K. Behera, S. A. Rao, H. Weng, and T. Yamagata (2007), El Niño Modoki and its possible teleconnection, *J. Geophys. Res.*, *112*, C11007, doi:10.1029/2006JC003798.

Baldwin, M., and K. E. Mitchell (1997), The NCEP hourly multi-sensor U.S. precipitation analysis for operations and GCIP research, paper presented at 13th AMS Conference on Hydrology, Am. Meteorol. Soc., Boston, Mass.

Bamston, A. G., M. Chelliah, and S. B. Goldenberg (1997), Documentation of a highly ENSO-related SST region in the equatorial Pacific: Research note, *Atmos. Ocean*, *35*(3), 367–383, doi:10.1080/07055900.1997.9649597.

Barlow, M., S. Nigam, and E. H. Berbery (2001), ENSO, Pacific decadal variability, and U.S. summertime precipitation, drought, and stream Flow, *J. Clim.*, *14*(9), 2105–2128, doi:10.1175/1520-0442(2001)014<2105:EPDVAU>2.0.CO;2.

Castro, C. L., T. B. McKee, and R. A. Pielke (2001), The relationship of the North American monsoon to tropical and North Pacific sea surface temperatures as revealed by observational analyses, *J. Clim.*, *14*(24), 4449–4473, doi:10.1175/1520-0442(2001)014<4449:TROTNA>2.0.CO;2.

Changnon, S. A., and G. D. Bell (2000), *El Niño, 1997–1998: The Climate Event of the Century*, Oxford Univ. Press, New York.

Chen, F., and J. Dudhia (2001), Coupling an advanced land surface–hydrology model with the Penn State–NCAR MM5 modeling system. Part I: Model Implementation and sensitivity, *Mon. Weather Rev.*, *129*(4), 569–585, doi:10.1175/1520-0493(2001)129<0569:CAALSH>2.0.CO;2.

Chen, F., K. Mitchell, J. Schaake, Y. Xue, H.-L. Pan, V. Koren, Q. Y. Duan, M. Ek, and A. Betts (1996), Modeling of land surface evaporation by four schemes and comparison with FIFE observations, *J. Geophys. Res.*, *101*(D3), 7251–7268, doi:10.1029/95JD02165.

Chen, J., and P. Kumar (2002), Role of terrestrial hydrologic memory in modulating ENSO impacts in North America, *J. Clim.*, *15*(24), 3569–3585, doi:10.1175/1520-0442(2003)015<3569:ROTHMI>2.0.CO;2.

Cole, J. E., J. T. Overpeck, and E. R. Cook (2002), Multiyear La Niña events and persistent drought in the contiguous United States, *Geophys. Res. Lett.*, *29*(13), 1647, doi:10.1029/2001GL013561.

Dahm, C. N., R. J. Edwards, and F. P. Gelwick (2005), Gulf Coast rivers of the southwestern United States, in *Rivers of North America*, edited by C. B. Arthur and E. C. Colbert, pp. 180–228, Academic, San Diego, Calif., doi:10.1016/B978-012088253-3/50008-0.

Daly, C., R. P. Neilson, and D. L. Phillips (1994), A statistical-topographic model for mapping climatological precipitation over mountainous terrain, *J. Appl. Meteorol.*, *33*(2), 140–158, doi:10.1175/1520-0450(1994)033<0140:ASTMFM>2.0.CO;2.

Delhomme, J. P. (1978), Kriging in the hydrosciences, *Adv. Water Resour.*, *1*(5), 251–266, doi:10.1016/0309-1708(78)90039-8.

Dirmeyer, P. A., A. J. Dolman, and N. Sato (1999), The pilot phase of the Global Soil Wetness Project, *Bull. Am. Meteorol. Soc.*, *80*(5), 851–878, doi:10.1175/1520-0477(1999)080<0851:TPPOTG>2.0.CO;2.

Goodrich, G. B. (2004), Influence of the Pacific Decadal Oscillation on Arizona winter precipitation during years of neutral ENSO, *Weather Forecast.*, *19*(5), 950–953, doi:10.1175/1520-0434(2004)019<0950:IOTPDO>2.0.CO;2.

Grinsted, A., J. C. Moore, and S. Jevrejeva (2004), Application of the cross wavelet transform and wavelet coherence to geophysical time series, *Nonlinear Process. Geophys.*, *11*(5/6), 561–566, doi:10.5194/npg-11-561-2004.

Hansen, M. C., R. S. Defries, J. R. G. Townshend, and R. Sohlberg (2000), Global land cover classification at 1 km spatial resolution using a classification tree approach, *Int. J. Remote Sens.*, *21*(6–7), 1331–1364, doi:10.1080/014311600210209.

Henderson-Sellers, A., K. McGuffie, and A. J. Pitman (1996), The Project for Intercomparison of Land-surface Parametrization Schemes (PILPS): 1992 to 1995, *Clim. Dyn.*, *12*(12), 849–859, doi:10.1007/s003820050147.

Higgins, R. W., Y. Yao, and X. L. Wang (1997), Influence of the North American monsoon system on the U.S. summer precipitation regime, *J. Clim.*, *10*(10), 2600–2622, doi:10.1175/1520-0442(1997)010<2600:IOTNAM>2.0.CO;2.

Hogue, T. S., L. Bastidas, H. Gupta, S. Sorooshian, K. Mitchell, and W. Emmerich (2005), Evaluation and transferability of the Noah Land Surface Model in semiarid environments, *J. Hydrometeorol.*, *6*(1), 68–84, doi:10.1175/JHM-402.1.

Intergovernmental Panel on Climate Change (2007), *Climate Change 2007: Impacts, Adaptation and Vulnerability. Contribution of Working Group II to the Fourth Assessment Report of the Intergovernmental Panel on Climate Change*, Cambridge Univ. Press, Cambridge, U. K.

International Boundary and Water Commission (1906), *Convention Between the United States and Mexico: Equitable Distribution of the Waters of the Rio Grande*, Gov. Printing Off., Washington, D. C.

Jacquemin, B., and J. Noilhan (1990), Sensitivity study and validation of a land surface parameterization using the HAPEX-MOBILHY data set, *Boundary Layer Meteorol.*, *52*(1–2), 93–134, doi:10.1007/BF00123180.

Joyce, R. J., J. E. Janowiak, P. A. Arkin, and P. Xie (2004), CMORPH: A method that produces global precipitation estimates from passive microwave and infrared data at high spatial and temporal resolution, *J. Hydrometeorol.*, *5*(3), 487–503, doi:10.1175/1525-7541(2004)005<0487:CAMTPG>2.0.CO;2.

Kahya, E., and J. A. Dracup (1993), U.S. streamflow patterns in relation to the El Niño/Southern Oscillation, *Water Resour. Res.*, *29*(8), 2491–2503, doi:10.1029/93WR00744.

Kaplan, A., M. A. Cane, Y. Kushnir, A. C. Clement, M. B. Blumenthal, and B. Rajagopalan (1998), Analyses of global sea surface temperature 1856–1991, *J. Geophys. Res.*, *103*(C9), 18,567–18,589, doi:10.1029/97JC01736.

Karl, T. R., C. N. Williams Jr., F. T. Quinlan, and T. A. Boden (1990), *United States Historical Climatology Network (HCN) Serial Temperature and Precipitation Data* Rep, 389 pp., Environ. Sci. Div., Carbon Dioxide Inf. and Anal. Cent., Oak Ridge Natl. Lab., Oak Ridge, Tenn.

Kiladis, G. N., and H. F. Diaz (1986), An analysis of the 1877–78 ENSO episode and comparison with 1982–83, *Mon. Weather Rev.*, *114*(6), 1035–1047, doi:10.1175/1520-0493(1986)114<1035:AAOTEE>2.0.CO;2.

Koren, V., J. Schaake, K. Mitchell, Q. Y. Duan, F. Chen, and J. M. Baker (1999), A parameterization of snowpack and frozen ground intended for NCEP weather and climate models, *J. Geophys. Res.*, *104*(D16), 19,569–19,585, doi:10.1029/1999JD900232.

Kumar, A., and M. P. Hoerling (2003), The nature and causes for the delayed atmospheric response to El Niño, *J. Clim.*, *16*(9), 1391–1403, doi:10.1175/1520-0442-16.9.1391.

Kumar, A., A. Leetmaa, and M. Ji (1994), Simulations of atmospheric variability induced by sea surface temperatures and implications for global warming, *Science*, *266*(5185), 632–634, doi:10.1126/science.266.5185.632.

Kumar, P., and E. Foufoula-Georgiou (1997), Wavelet analysis for geophysical applications, *Rev. Geophys.*, *35*(4), 385–412, doi:10.1029/97RG00427.

Kumar, S. V., et al. (2006), Land information system: An interoperable framework for high resolution land surface modeling, *Environ. Model. Software*, *21*(10), 1402–1415, doi:10.1016/j.envsoft.2005.07.004.

Kurtzman, D., and B. R. Scanlon (2007), El Niño–Southern Oscillation and Pacific Decadal Oscillation impacts on precipitation in the southern and central United States: Evaluation of spatial distribution and predictions, *Water Resour. Res.*, *43*, W10427, doi:10.1029/2007WR005863.

Labat, D., R. Ababou, and A. Mangin (2001), Introduction of wavelet analyses to rainfall/runoffs relationship for a karstic basin: The case of Licq-Atherey karstic system (France), *Ground Water*, *39*(4), 605–615, doi:10.1111/j.1745-6584.2001.tb02348.x.

Larkin, N. K., and D. E. Harrison (2005), On the definition of El Niño and associated seasonal average U.S. weather anomalies, *Geophys. Res. Lett.*, *32*, L13705, doi:10.1029/2005GL022738.

Lau, K.-M., and H. Weng (1995), Climate signal detection using wavelet transform: How to make a time series sing, *Bull. Am. Meteorol. Soc.*, *76*(12), 2391–2402, doi:10.1175/1520-0477(1995)076<2391:CSDUWT>2.0.CO;2.

Legates, D. R., H. F. Lins, and G. J. McCabe (2005), Comments on "Evidence for global runoff increase related to climate warming" by Labat et al., *Adv. Water Resour.*, *28*(12), 1310–1315, doi:10.1016/j.advwatres.2005.04.006.

Lohmann, D., et al. (2004), Streamflow and water balance intercomparisons of four land surface models in the North American Land Data Assimilation System project, *J. Geophys. Res.*, *109*, D07S91, doi:10.1029/2003JD003517.

Luo, L., et al. (2003), Validation of the North American Land Data Assimilation System (NLDAS) retrospective forcing over the southern Great Plains, *J. Geophys. Res.*, *108*(D22), 8843, doi:10.1029/2002JD003246.

Mahfouf, J. F., and J. Noilhan (1991), Comparative study of various formulations of evaporations from bare soil using in situ data, *J. Appl. Meteorol.*, *30*(9), 1354–1365, doi:10.1175/1520-0450(1991)030<1354:CSOVFO>2.0.CO;2.

Mahrt, L., and M. Ek (1984), The influence of atmospheric stability on potential evaporation, *J. Clim. Appl. Meteorol.*, *23*(2), 222–234, doi:10.1175/1520-0450(1984)023<0222:TIOASO>2.0.CO;2.

Mahrt, L., and H. Pan (1984), A two-layer model of soil hydrology, *Boundary Layer Meteorol.*, *29*(1), 1–20, doi:10.1007/BF00119116.

Mantua, N., and S. Hare (2002), The Pacific Decadal Oscillation, *J. Oceanogr.*, *58*(1), 35–44, doi:10.1023/A:1015820616384.

Mantua, N. J., S. R. Hare, Y. Zhang, J. M. Wallace, and R. C. Francis (1997), A Pacific interdecadal climate oscillation with impacts on salmon production, *Bull. Am. Meteorol. Soc.*, *78*(6), 1069–1079, doi:10.1175/1520-0477(1997)078<1069:APICOW>2.0.CO;2.

McCabe, G. J., and M. D. Dettinger (1999), Decadal variations in the strength of ENSO teleconnections with precipitation in the western United States, *Int. J. Climatol.*, *19*(13), 1399–1410, doi:10.1002/(SICI)1097-0088(19991115)19:13<1399::AID-JOC457>3.0.CO;2-A.

McRoberts, D. B., and J. W. Nielsen-Gammon (2011), A new homogenized climate division precipitation data set for analysis of climate variability and climate change, *J. Appl. Meteorol. Climatol.*, *50*, 1187–1199, doi:10.1175/2010JAMC2626.1

Mesinger, F., et al. (2006), North American Regional Reanalysis, *Bull. Am. Meteorol. Soc.*, *87*(3), 343–360, doi:10.1175/BAMS-87-3-343.

Minobe, S. (1997), A 50–70 year climatic oscillation over the North Pacific and North America, *Geophys. Res. Lett.*, *24*(6), 683–686, doi:10.1029/97GL00504.

Mitchell, K. E. (2005), The Community Noah Land-surface model: User's guide, public release version 2.7.1, report, 26 pp., Environ. Model. Cent., NOAA, Silver Spring, Md.

Mitchell, K. E., et al. (2004), The multi-institution North American Land Data Assimilation System (NLDAS): Utilizing multiple GCIP products and partners in a continental distributed hydrological modeling system, *J. Geophys. Res.*, *109*, D07S90, doi:10.1029/2003JD003823.

Namias, J. (1966), Nature and possible causes of the northeastern United States drought during 1962–65, *Mon. Weather Rev.*, *94*(9), 543–554, doi:10.1175/1520-0493(1966)094<0543:NAPCOT>2.3.CO;2.

Namias, J. (1967), Further studies of drought over the northeastern United States, *Mon. Weather Rev.*, *95*(8), 497–508, doi:10.1175/1520-0493(1967)095<0497:FSODON>2.3.CO;2.

Neelin, J. D. (2010), *Climate Change and Climate Modeling*, Cambridge Univ. Press, Cambridge, U. K.

Newman, M., G. P. Compo, and M. A. Alexander (2003), ENSO-forced variability of the Pacific Decadal Oscillation, *J. Clim.*, *16*(23), 3853–3857, doi:10.1175/1520-0442(2003)016<3853:EVOTPD>2.0.CO;2.

Noilhan, J., and S. Planton (1989), A simple parameterization of land surface processes for meteorological models, *Mon. Weather Rev.*, *117*(3), 536–549, doi:10.1175/1520-0493(1989)117<0536:ASPOLS>2.0.CO;2.

O'Brien, J. (2002), Definition(s) of La Niña, in *La Niña and Its Impacts: Facts and Speculation*, edited by M. H. Glantz, pp. 31–38, U. N. Univ. Press, Tokyo.

Özger, M., A. K. Mishra, and V. P. Singh (2009), Low frequency drought variability associated with climate indices, *J. Hydrol.*, *364*(1–2), 152–162, doi:10.1016/j.jhydrol.2008.10.018.

Pan, H. L., and L. Mahrt (1987), Interaction between soil hydrology and boundary-layer development, *Boundary Layer Meteorol.*, *38*(1–2), 185–202, doi:10.1007/BF00121563.

Pan, M., et al. (2003), Snow process modeling in the North American Land Data Assimilation System (NLDAS): 2. Evaluation of model simulated snow water equivalent, *J. Geophys. Res.*, *108*(D22), 8850, doi:10.1029/2003JD003994.

Patiño-Gomez, C. (2005), *GIS for Large-Scale Watershed Observational Data Model*, 282 pp., Univ. of Tex. at Austin, Austin.

Patten, J. M., S. R. Smith, and J. J. O'Brien (2003), Impacts of ENSO on snowfall frequencies in the United States, *Weather Forecast.*, *18*(5), 965–980, doi:10.1175/1520-0434(2003)018<0965:IOEOSF>2.0.CO;2.

Peters-Lidard, C., et al. (2007), High-performance Earth system modeling with NASA/GSFC's Land Information System, *Innov. Systems Software Eng.*, *3*(3), 157–165, doi:10.1007/s11334-007-0028-x.

Piechota, T. C., and J. A. Dracup (1996), Drought and regional hydrologic variation in the United States: Associations with the El Niño–Southern Oscillation, *Water Resour. Res.*, *32*(5), 1359–1373, doi:10.1029/96WR00353.

Pielke, R. A., and C. N. Landsea (1999), La Niña, El Niño and Atlantic hurricane damages in the United States, *Bull. Am. Meteorol. Soc.*, *80*(10), 2027–2033, doi:10.1175/1520-0477(1999)080<2027:LNAENO>2.0.CO;2.

Quiring, S., and G. Goodrich (2008), Nature and causes of the 2002 to 2004 drought in the southwestern United States compared with the historic 1953 to 1957 drought, *Clim. Res.*, *36*(1), 41–52, doi:10.3354/cr00735.

Rasmusson, E. M., and T. H. Carpenter (1982), Variations in tropical sea surface temperature and surface wind fields associated with the Southern Oscillation/El Niño, *Mon. Weather Rev.*, *110*(5), 354–384, doi:10.1175/1520-0493(1982)110<0354:VITSST>2.0.CO;2.

Redmond, K. T., and R. W. Koch (1991), Surface Climate and streamflow variability in the western United States and their relationship to large-scale circulation indices, *Water Resour. Res.*, *27*(9), 2381–2399, doi:10.1029/91WR00690.

Revenga, C., J. Nackoney, E. Hoshino, Y. Kura, and J. Maidens (2003), *Watersheds of the World*, World Resour. Inst., Washington, D. C.

Rivera, N., S. Ray, J. Jensen, A. Chan, and W. Ayers (2004), Detection of cyclic patterns using wavelets: An example study in the Ormskirk Sandstone, Irish Sea, *Math. Geol.*, *36*(5), 529–543, doi:10.1023/B:MATG.0000037735.34280.42.

Robock, A., et al. (2003), Evaluation of the North American Land Data Assimilation System over the southern Great Plains during the warm season, *J. Geophys. Res.*, *108*(D22), 8846, doi:10.1029/2002JD003245.

Rodell, M., et al. (2004), The Global Land Data Assimilation System, *Bull. Am. Meteorol. Soc.*, *85*(3), 381–394, doi:10.1175/BAMS-85-3-381.

Ropelewski, C. F., and M. S. Halpert (1986), North American precipitation and temperature patterns associated with the El Niño/Southern Oscillation (ENSO), *Mon. Weather Rev.*, *114*(12), 2352–2362, doi:10.1175/1520-0493(1986)114<2352:NAPATP>2.0.CO;2.

Sahoo, A. K., P. A. Dirmeyer, P. R. Houser, and M. Kafatos (2008), A study of land surface processes using land surface models over the Little River Experimental Watershed, Georgia, *J. Geophys. Res.*, *113*, D20121, doi:10.1029/2007JD009671.

Sandoval-Solis, S., D. C. McKinney, R. L. Teasley, and J. Schuldes (2010), Memo: Comparison of annual naturalized flows for the Rio Grande/Rio Bravo basin: TCEQ-CONAGUA, report, Cent. for Res. in Water Resour., Bur. of Eng. Res., Univ. of Tex. at Austin, Austin.

Schaake, J. C., V. I. Koren, Q.-Y. Duan, K. Mitchell, and F. Chen (1996), Simple water balance model for estimating runoff at different spatial and temporal scales, *J. Geophys. Res.*, *101*(D3), 7461–7475, doi:10.1029/95JD02892.

Schaake, J. C., et al. (2004), An intercomparison of soil moisture fields in the North American Land Data Assimilation System (NLDAS), *J. Geophys. Res.*, *109*, D01S90, doi:10.1029/2002JD003309.

Schoennagel, T., T. T. Veblen, W. H. Romme, J. S. Sibold, and E. R. Cook (2005), ENSO and PDO variability affect drought-induced fire occurrence in Rocky Mountain subalpine forests, *Ecol. Appl.*, *15*(6), 2000–2014, doi:10.1890/04-1579.

Sheffield, J., et al. (2003), Snow process modeling in the North American Land Data Assimilation System (NLDAS): 1. Evaluation of model-simulated snow cover extent, *J. Geophys. Res.*, *108*(D22), 8849, doi:10.1029/2002JD003274.

Shukla, S., and A. W. Wood (2008), Use of a standardized runoff index for characterizing hydrologic drought, *Geophys. Res. Lett.*, *35*, L02405, doi:10.1029/2007GL032487.

Smith, S. R., and J. J. O'Brien (2001), Regional snowfall distributions associated with ENSO: Implications for seasonal forecasting, *Bull. Am. Meteorol. Soc.*, *82*(6), 1179–1191, doi:10.1175/1520-0477(2001)082<1179:RSDAWE>2.3.CO;2.

Torrence, C., and G. P. Compo (1998), A practical guide to wavelet analysis, *Bull. Am. Meteorol. Soc.*, *79*(1), 61–78, doi:10.1175/1520-0477(1998)079<0061:APGTWA>2.0.CO;2.

Trenberth, K. E. (1990), Recent observed interdecadal climate changes in the Northern Hemisphere, *Bull. Am. Meteorol. Soc.*, *71*(7), 988–993, doi:10.1175/1520-0477(1990)071<0988:ROICCI>2.0.CO;2.

Trenberth, K. E. (1997), The definition of El Niño, *Bull. Am. Meteorol. Soc.*, *78*(12), 2771–2777, doi:10.1175/1520-0477(1997)078<2771:TDOENO>2.0.CO;2.

Trenberth, K. E., and T. J. Hoar (1996), The 1990–1995 El Niño–Southern oscillation event: Longest on record, *Geophys. Res. Lett.*, *23*(1), 57–60, doi:10.1029/95GL03602.

U.S. Army Corps of Engineers (2008), Forgotten reach of the Rio Grande, Fort Quitman to Presidio, Texas, report, 169 pp., Tex. Comm. on Environ. Qual., Albuquerque, N. M.

von Storch, H., and F. W. Zwiers (2003), *Statistical Analysis in Climate Research*, Cambridge Univ. Press, Cambridge, U. K.

Weng, H., K. Ashok, S. Behera, S. Rao, and T. Yamagata (2007), Impacts of recent El Niño Modoki on dry/wet conditions in the Pacific Rim during boreal summer, *Clim. Dyn.*, *29*(2–3), 113–129, doi:10.1007/s00382-007-0234-0.

Wolf, A. T. (2002), *Atlas of International Freshwater Agreements*, U. N. Environ. Programme, Nairobi.

Wolter, K., and M. S. Timlin (1993), Monitoring ENSO in COADS with a seasonally adjusted principal component index, paper presented at 17th Climate Diagnostics Workshop, Univ. of Okla., Norman.

Wolter, K., and M. S. Timlin (1998), Measuring the strength of ENSO events—How does 1997/98 rank?, *Weather*, *53*, 315–324.

Woolhiser, D. A., T. O. Keefer, and K. T. Redmond (1993), Southern oscillation effects on daily precipitation in the southwestern United States, *Water Resour. Res.*, *29*(4), 1287–1295, doi:10.1029/92WR02536.

Wurbs, R. A. (2006), Methods for developing naturalized monthly flows at gaged and ungaged sites, *J. Hydrol. Eng.*, *11*(1), 55–64, doi:10.1061/(ASCE)1084-0699(2006)11:1(55).

Zhang, Y., J. M. Wallace, and D. S. Battisti (1997), ENSO-like interdecadal variability: 1900–93, *J. Clim.*, *10*(5), 1004–1020, doi:10.1175/1520-0442(1997)010<1004:ELIV>2.0.CO;2.

Zobler, L. (1986), A world soil file for global climate modelling, report, NASA Goddard Inst. for Space Stud., New York.

H. K. Beaudoing, Earth System Science Interdisciplinary Center, University of Maryland, College Park, MD 20740, USA. (hiroko.kato-1@nasa.gov)

J. D. Bolten, Hydrologic Science Branch, NASA Goddard Space Flight Center, Code 614.3, Bldg. 33, Greenbelt, MD 20771, USA. (john.bolten@nasa.gov)

J. R. Giardino, Department of Geology and Geophysics, Texas A&M University, 257 Halbouty, MS 3115, College Station, TX 77843, USA. (rickg@tamu.edu)

R. A. Kaiser, Department of Recreation, Park and Tourism Sciences, Texas A&M University, Agriculture and Life Sciences Bldg., Ste. 409K, 600 John Kimbrough Blvd., MS 2261, College Station, TX 77843, USA. (rkaiser@tamu.edu)

C. P. Khedun, Water Management and Hydrological Science, Texas A&M University, 321 Scoates Hall, MS 2117, College Station, TX 77843, USA. (pkhedun@tamu.edu)

A. K. Mishra, Department of Biological and Agricultural Engineering, Texas A&M University, 321 Scoates Hall, MS 2117, College Station, TX 77843, USA. (akm.pce@gmail.com)

V. P. Singh, Department of Civil Engineering, Texas A&M University, 321 Scoates Hall, MS 2117, College Station, TX 77843, USA. (vsingh@tamu.edu)